

The interaction of lncRNA EZR-AS1 with SMYD3 maintains overexpression of EZR in ESCC cells

Xiao-Dan Zhang^{1,2,3}, Guo-Wei Huang^{1,4}, Ying-Hua Xie^{1,2}, Jian-Zhong He^{1,4}, Jin-Cheng Guo^{1,2}, Xiu-E Xu^{1,4}, Lian-Di Liao^{1,4}, Yang-Min Xie^{1,5}, Yong-Mei Song⁶, En-Min Li^{1,2,*} and Li-Yan Xu^{1,4,*}

¹The Key Laboratory of Molecular Biology for High Cancer Incidence Coastal Chaoshan Area, Medical College of Shantou University, Shantou 514041, Guangdong, PR China, ²Department of Biochemistry and Molecular Biology, Medical College of Shantou University, Shantou 514041, Guangdong, PR China, ³The Affiliated Nanshan People's Hospital of Shenzhen University, Shenzhen Municipal Sixth People's Hospital, Shenzhen 518060, Guangdong, PR China, ⁴Institute of Oncologic Pathology, Medical College of Shantou University, Shantou 514041, Guangdong, PR China, ⁵Department of Experimental Animal Center, Medical College of Shantou University, Shantou 515041, PR China and ⁶State Key Laboratory of Molecular Oncology, Cancer Institute and Cancer Hospital, Chinese Academy of Medical Sciences and Peking Union Medical College, Beijing 100021, PR China

Received September 29, 2016; Revised December 01, 2017; Editorial Decision December 05, 2017; Accepted December 05, 2017

ABSTRACT

EZR, a member of the ezrin-radixin-moesin (ERM) family, is involved in multiple aspects of cell migration and cancer. SMYD3, a histone H3–lysine 4 (H3–K4)-specific methyltransferase, regulates EZR gene transcription, but the molecular mechanisms of epigenetic regulation remain ill-defined. Here, we show that antisense lncRNA EZR-AS1 was positively correlated with EZR expression in both human esophageal squamous cell carcinoma (ESCC) tissues and cell lines. Both *in vivo* and *in vitro* studies revealed that EZR-AS1 promoted cell migration through up-regulation of EZR expression. Mechanistically, antisense lncRNA EZR-AS1 formed a complex with RNA polymerase II to activate the transcription of EZR. Moreover, EZR-AS1 could recruit SMYD3 to a binding site, present in a GC-rich region downstream of the EZR promoter, causing the binding of SMYD3 and local enrichment of H3K4me3. Finally, the interaction of EZR-AS1 with SMYD3 further enhanced EZR transcription and expression. Our findings suggest that antisense lncRNA EZR-AS1, as a member of an RNA polymerase complex and through enhanced SMYD3-dependent H3K4 methylation, plays an important role in enhancing transcription of the EZR gene to promote the mobility and invasiveness of human cancer cells.

INTRODUCTION

Global transcriptional analyses have demonstrated that mammalian genomes contain large numbers of long non-coding RNAs (lncRNAs), which are longer than 200 nt and do not encode proteins (1–7). Among these, antisense lncRNAs are defined as lncRNAs transcribed from the antisense strand of well-defined transcriptional units (8,9). Though most lncRNAs are expressed at levels lower than protein-coding transcripts, antisense lncRNAs play important roles in regulating gene expression. In recent years, significant insight has been gained into the molecular mechanisms by which antisense lncRNAs function (10,11). Among these, interaction with proteins is one of the most common ways. Antisense lncRNAs interact with transcription factors (12), chromatin remodelers (13) and histone methylases and demethylases (14,15), and thus participate in all stages of gene expression (10,16,17), from transcription to translation (18,19).

Ezrin (EZR), a member of the ezrin-radixin-moesin (ERM) family of cytoskeletal proteins, links the actin cytoskeleton to the plasma membrane. Through modulation of the cytoskeleton and as a regulator of signaling molecules, EZR participates in many cellular processes essential for normal growth, such as adhesion, cell polarity and migration, cytokinesis, and formation of surface structures (20–23). Since EZR overexpression in many human cancers promotes cell migration, correlates with poor prognosis and is a therapeutic target, we and others have been prompted to identify the key molecules involved in EZR regulation (24–33).

*To whom correspondence should be addressed. Tel: +86 754 88900460; Fax: +86 754 88900847; Email: lyxu@stu.edu.cn
Correspondence may also be addressed to Dr. En-Min Li. Email: nmli@stu.edu.cn

EZR, encoded by the *VIL2* gene, has two transcript variants—variant 1 (V1) and variant 2 (V2)—that differ in their transcriptional start sites, but encode the same protein (Figure 1A). Many cytokines can up-regulate (e.g. interleukin 11 and tumor necrosis factor alpha) or down-regulate (e.g. interleukin 2) EZR expression (34–36). In a previous study, we found that specificity protein 1 (SP1) and activator protein 1 (AP-1, a c-Jun/c-Fos heterodimer) binding sites serve as promoter elements for basal transcription of the EZR gene, as well as a composite 12-*O*-tetradecanoylphorbol-13-acetate (TPA)-responsive element for EZR transcription in ESCC cells (35,37). Moreover, epigenetic reprogramming of histone modifications increases EZR expression through histone modification (i.e. tri-methyl-histone 3-K4) within the promoter region for EZR (38), in part through the histone modifier SET and MYND domain-containing 3 (SMYD3) (39). However, the molecular mechanisms regulating SMYD3 binding to the EZR promoter have not been identified.

From the UCSC Genome Browser (<http://genome.ucsc.edu/>) (40), we identified a natural antisense lncRNA, which we denote EZR antisense AS1 (EZR-AS1), which is transcribed from the opposite strand in the EZR gene locus, contains three exons and overlaps with EZR, spanning the first intron and first exon of the EZR variant 1 transcript (Figure 1A and Supplementary Figure S1). However, little is known concerning whether EZR and EZR-AS1 are related in terms of expression and function. More importantly, in the event of a correlation, it would remain unclear how EZR-AS1 could regulate the expression and function of EZR.

MATERIALS AND METHODS

Reagents, antibodies and constructs

The *firefly* luciferase-expressing plasmids pGL3-Basic (pGLB) and pGL3-Promoter (pGLP), and *Renilla* luciferase-expressing plasmid pRL-TK were purchased from Promega. Antibody against EZR (MS-661-P1, mouse monoclonal antibody) was purchased from Neomarker. Anti-SMYD3 antibody-ChIP Grade (ab85277, rabbit monoclonal antibody), anti-RNA polymerase II antibody-ChIP Grade (ab26721, rabbit monoclonal antibody), anti-SP1 antibody-ChIP Grade (ab13370, rabbit monoclonal antibody) and anti-Histone H3 (tri-methyl K4) (H3K4me3) antibody-ChIP Grade (ab213224, rabbit monoclonal antibody) were purchased from Abcam. Antibodies against β -actin (sc-47778, mouse monoclonal antibody), β -tubulin (sc-23949, mouse monoclonal antibody) and EGFP (sc-9996, mouse monoclonal antibody) were purchased from Santa Cruz Biotechnology. Anti-Flag M2 monoclonal antibody (F3165) was from Sigma. All other reagents were of analytical reagent grade. pGLB-hE(-1324/+134), pGLB-hE(-697/+134) and pGLB-hE(-87/-134) luciferase reporter plasmids, and pCMV, pCMV-SP1 and pCMV-C-Jun plasmids were described in our previous work (37). pGLB-hE(-1324/+550), pGLB-hE(-87/+550), and pGLB-hE(-1324/+134-mSBS2), pGLB-hE(-697/+134-mSBS2) and pGLB-hE(-1324/+550-mSBS2) with a mutated SMYD3 binding

site-2, and pGLB-hE(-1324/+550-mSBS1) and pGLB-hE(-87/+550-mSBS1), both with a mutated SMYD3 binding site-1, were synthesized by GENEWIZ (Suzhou, China). Plasmids with mutated SMYD3 binding sites were constructed by replacing CCCTCC with ATAGAA. Full-length EZR-AS1 (NR_102425.1, 362 bp) and EZR-AS1 antisense were also synthesized by GENEWIZ and cloned into the pcDNA3.1 vector (Invitrogen). EZR-AS1/1–137, EZR-AS1/1–281, EZR-AS1/131–281, and EZR-AS1/131–362 were generated by polymerase chain reaction (PCR), using primers shown in Table 1, and sub-cloned into pcDNA3.1. SMYD3/1–428, SMYD3/40–428, SMYD3/100–428, SMYD3/250–428 and SMYD3/1–250 constructs were cloned into a pcDNA3.1-Flag vector using primers shown in Table 1.

ESCC tissue specimens

We collected paired tumor and adjacent normal tissues from 30 patients who underwent surgical resection, for ESCC, at the Shantou Central Hospital between 2012 and 2013. After being examined by a pathologist, tissues were immediately frozen in liquid nitrogen and stored at -80°C . Transcriptome sequencing (RNA-seq) of 15 pairs of human ESCC tissues and pair-matched normal esophageal tissues was performed by the Shanghai Biotechnology Corporation. Transcriptome sequencing data are available publicly at the Sequence Read Archive (<http://www.ncbi.nlm.nih.gov/sra/>) under accession number SRP064894 (41). Written informed consent was obtained from all patients or their appropriate surrogates. This study was approved by the ethics committees of Shantou Central Hospital and Shantou University Medical College.

Cell culture, plasmid transfection and RNA interference

Cell lines used in this study and related cell culture general information have been described previously (35). Briefly, KYSE150 and KYSE510 esophageal carcinoma cells were maintained in RPMI 1640 medium (Thermo Scientific) containing 10% fetal bovine serum (Thermo Scientific), penicillin-G (100 units/ml) and streptomycin (100 $\mu\text{g/ml}$), and incubated at 37°C in a humidified atmosphere containing 5% CO_2 . KYSE150 and KYSE510 cells were seeded into plates and cultured for 12–24 h until 70–80% confluence. Plasmids were transfected into KYSE150 or KYSE510 cells using Lipofectamine 3000 (Invitrogen). Then cells were cultured and used for further analysis.

EZR-AS1 siRNAs were targeted to the non-overlapping domain between EZR and EZR-AS1, specifically siEZR-AS1-1 is located within the third exon of EZR-AS1, while siEZR-AS1-2 stretched across the second and third exons of EZR-AS1 (Figure 1A). Both siRNAs were synthesized by GenePharma (Suzhong, Jiangsu, China), as was the scrambled siRNA (NC). ESCC cells were transfected with 30 nM siRNA using Lipofectamine 3000 (Invitrogen) according to the manufacturer's instructions, and harvested at 48 h post-transfection. When transfecting both EZR-AS1 siRNAs 1 and 2 together, we transfected 15 nM of each EZR-AS1 siRNA. When transfecting either EZR-AS1 siRNA 1 or 2, 15

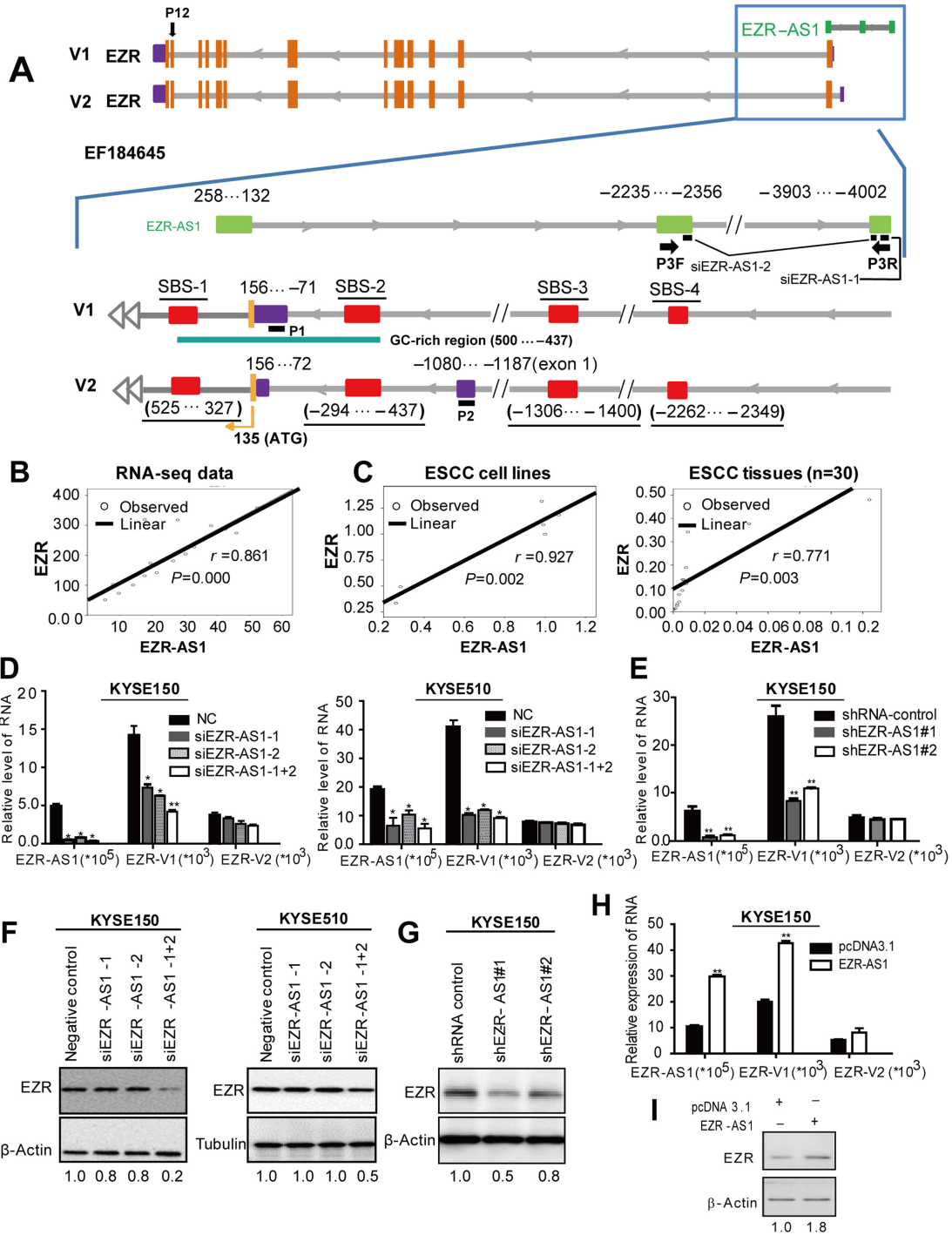


Figure 1. EZR and EZR-AS1 expression are positively correlated, and EZR-AS1 up-regulates EZR expression. (A) Schematic represents the genomic structure of antisense lncRNA EZR-AS1 and protein-coding gene EZR. Human EZR-AS1 is *cis*-transcribed from the opposite strand of the human EZR gene on chromosome 6. Exons of EZR-AS1 and EZR are depicted as green and orange boxes, respectively, and untranslated regions of EZR are purple; introns are shown in grey. The arrowhead represents the orientation of the sequences. Red represents SMYD3 binding sites (SBSs). P1, P2 and P12 represent qRT-PCR primers for EZR variant 1 (V1), variant 2 (V2) and exon 12 of EZR, respectively. (B) RNA-seq was used to detect the relationship between EZR-AS1 and EZR expression in 15 pairs of ESCC samples. (C) qRT-PCR detection of EZR-AS1 and EZR expression in 7 ESCC cell lines and 30 pairs of additional ESCC tissues. Data are representative of at least two independent experiments. (D) qRT-PCR detection of EZR-AS1, EZR-V1 and EZR-V2 expression in KYSE150 and KYSE510 cells in which EZR-AS1 expression was silenced by two different siRNAs. (E) EZR-AS1, EZR-V1 or EZR-V2 was detected by qRT-PCR in KYSE150 cells following stable knockdown of EZR-AS1. (F) Western blot analysis of EZR protein in KYSE150 and KYSE510 cells transfected with siRNAs against EZR-AS1. (G) Western blot analysis of EZR protein in KYSE150 cells following stable knockdown of EZR-AS1. (H) qRT-PCR detection of EZR-AS1, EZR-V1 or EZR-V2 in KYSE150 cells transiently transfected with EZR-AS1 or pcDNA3.1. (I) Western blot analysis of EZR protein in KYSE150 cells following transient transfection with EZR-AS1 or pcDNA3.1. Data represent the mean \pm SD ($n = 3$). All graphs in (A) to (I) represent data from three independent transfection experiments. * $P < 0.05$ or ** $P < 0.01$.

Table 1. Primers used in this study

Primer	Sequence	Names of construct
Primers for EZR-AS1 constructs		
EZR-AS1-1F	5'-CGCGGATCCAAGAACCCTGTTCCCCAGG-3'	
EZR-AS1-131F	5'-CGCGGATCCCACACTGCTGTTTGGGCAAC-3'	EZR-AS1/131-281
AS-137R	5'-CCGGAATTCCAGTGTGTCCAGAAACCG-3'	EZR-AS1/1-137
AS-281R	5'-CCGGAATTCTCCAAGTTGGCTGATTCCA-3'	EZR-AS1/1-281
AS-348R	5'-CCGGAATTCTTCTGTATTGGATTTTATTGGT-3'	EZR-AS1/131-348
Primers for SMYD3 constructs		
SMYD3-126F	5'-CTCGAGATGGAGCCGCTGAAGGTGG-3'	SMYD3/1-428
SMYD3-243F	5'-CTCGAGGTGTGCAAGGGGAGTCGTG-3'	SMYD3/40-428
SMYD3-426F	5'-CTCGAGTCCGTTTCGACTTCTTGGCAGAG-3'	SMYD3/100-428
SMYD3-876F	5'-CTCGAGAAGCAGCTGAGGGACCAGTAC-3'	SMYD3/250-428
SMYD3-1409R	5'-GAATTCGGATGCTGTGATGTTGGCGTC-3'	
SMYD3-876R	GAATTCGTAAGTCCCTCAGCTGCTT	SMYD3/1-250
Primers for qRT-PCR		
EZR1Q-F (P1)	5'-GCGGGCGCTCTAAGGGTTCT-3'	
EZR1Q-R (P1)	5'-ACTCGACATTGATTGGTTTCGGC-3'	
EZR2Q-F (P2)	5'-CTTTTGGGAGCGCGGGCAGC-3'	
EZR2Q-R (P2)	5'-AGACGCTGTCCAACCCGGC-3'	
EZR-exon 12-F	5'-GACCTGGTGAAGACCAAGGAG-3'	
EZR-exon 12-R	5'-CGCTCGTTCCTCTCTGCCTC-3'	
AS-131qF (P3F)	5'-CACACTGCTGTTTGGGCAAC-3'	
AS-281qR (P3R)	5'-TCCAAGGTTGGCTGATTCCA-3'	
F-ACTB	5'-CAACTGGGACGACATGGAGAAA-3'	
R-ACTB	5'-GATAGCAACGTACATGGCTGGG-3'	
Primers for ChIP		
EZR-SF1	GAGGTCAAAATCTCAGAAGAGGC	SBS1
EZR-SR1	CTCCCACTTGCAGATCCAGG	
EZR-SF2	GTCCAGCGATTCCCCCAAG	SBS2
EZR-SR2	AAGTGGGGAGGCTGTTTGTG	
EZR-SF3	CCCCTCTTCTCCGCCTCT	SBS3
EZR-SR3	CTCAGTGGGGAGGATCGG	
EZR-SF4	GTGGAGCGTTAGGAAAACACC	SBS4
EZR-SR4	CGGAAGCCATCTGAGTCTCC	
EZR-1578F	GACCTGGTGAAGACCAAGGAG	1792/1578
EZR-1792R	CGCTCGTTCCTCTGCCTC	
EZR-24F	GCCCCAACACCTCGAGC	140/24
EZR-140R	CAGCAGTGTGTCCAGAAAC	
EZR-885F	CTCAGTCTCTCCCGAAGG	-805/-804
EZR-804R	TCAAAAACCTGCAACCGCTCG	
F-ACTB	5'-CAACTGGGACGACATGGAGAAA-3'	423/600
R-ACTB	5'-GATAGCAACGTACATGGCTGGG-3'	

F: forward primer; R: reverse primer.
Restriction sites are underlined.

nM of the EZR-AS1 siRNA was combined with 15 nM scrambled siRNA so that a total of 30 nM siRNA was transfected. The two siRNA oligonucleotide sequences were as follows: EZR-AS-siRNA-1 (*Homo sapiens*), 5'-UAAUUUCCAAAUCUUUUCC-3'; EZR-AS-siRNA-2 (*Homo sapiens*), 5'-UGUAGAACCUGAAUAGAGG-3'. For SMYD3 siRNA, the two siRNA oligonucleotide sequences were as follows: SMYD3-siRNA-1 (*H. sapiens*), 5'-AGUAUCUCUUUGCUCUAAUC-3'; SMYD3-siRNA-2 (*H. sapiens*), 5'-CAAGUAUGGAAGGAAGUUC-3'. Small hairpin RNA lentiviruses for EZR-AS1 and SMYD3 were purchased from GenePharma of China. The shRNA sequences were identical to the siRNAs and were ligated into the pGLV3/H1/GFP/+Puro Vector. The lentiviruses encoding shRNAs were used to simultaneously infect ESCC cells, following the manufacturer's instructions, when cells reached 30% to 40% confluence. Seventy-two hours later, cells were harvested for further analysis or selected in puromycin to established stable cell line.

RNA purification and qRT-PCR analysis

Total RNA from ESCC tissue samples or ESCC cells was isolated with TRIzol (Invitrogen) as per the manufacturer's instructions, and the concentration determined by a Nanodrop (Agilent). One microgram total RNA was reverse-transcribed into cDNA by a Reverse Transcription System (Promega) according to the manufacturer's protocol. Quantitative real-time PCR (qRT-PCR) was performed by GoTaq[®] qPCR Master Mix (Promega) using a 7500 Real-Time PCR System (Applied Biosystems). Primer pairs for target genes used in the PCR assay are described in Table 1. β -Actin was measured as an internal control and used for normalization. RNA expression was normalized against the relative value from the NC control group. All experiments were replicated at least three times with $n = 4$ samples per experiment.

For cytoplasmic RNA and nuclear RNA separation assays, cells were washed twice with cold PBS and gently resuspended in hypotonic buffer (20 mM Tris-HCl, pH 7.4, 10 mM NaCl, 3 mM MgCl₂). Then NP40 was added to a final

concentration of 0.5% and the cell suspension was vortexed for 10 s, then centrifuged at 3000 rpm for 10 min at 4°C. The supernatant, representing the cytosol, was collected and an equal volume of chloroform was added, followed by centrifugation for 10 min at 4°C. The upper aqueous phase was transferred to a clean tube, and cytoplasmic RNA was isolated by mixing with an equal volume of ethanol according to the manufacturer's instructions. The nuclear pellet was resuspended and washed once with cold PBS, then centrifuged for 10 min at 4°C. The supernatant was discarded, and 1 ml Trizol was added to extract nuclear RNA. U6 small nuclear RNA (snRNA) and GAPDH mRNA were used as internal controls.

For RNase protection assays, cells were handled as previously described (42). Briefly, cells were collected by centrifugation and permeabilized in PBT (PBS; 0.05% Tween 20), then treated with 1000 U/ml RNase A, 1000 U/ml RNase H (Takara) or 1000 U/ml RNase inhibitor for 8 h at 25°C. RNA was then isolated with TRIzol (Invitrogen), and subsequently analyzed by qRT-PCR.

Western blotting

Cells were washed with ice-cold PBS, lysed on ice in RIPA buffer containing 1× complete protease inhibitor cocktail (Roche) and sonicated. The protein content in the lysates was detected using a BCA protein assay kit (Bio-Rad). Protein from Nude/Nude mice tissue samples was also isolated with RIPA buffer. Then equal amounts of whole cell extracts or tissue extracts were boiled at 100°C for 10 min in loading buffer, and were resolved by 10% SDS-polyacrylamide gel electrophoresis, using standard methodology, followed by transfer to a PVDF membrane (Roche). Blots were incubated with antibodies against EZR (1:500 dilution), SMYD3 (1:1000 dilution), RNA polymerase II (1:1000 dilution), SP1 (1:1000 dilution), β -actin (1:4000 dilution), β -tubulin (1:1000 dilution), EGFP (1:1000 dilution) and Flag-tag (1:10 000 dilution). Signals were detected, with luminol reagent, using a ChemiDoc Touch (Bio-Rad).

Dual-luciferase reporter assay

Cells were co-transfected with a reporter *firefly* luciferase-expressing plasmid (1 μ g), and a *Renilla* luciferase-expressing plasmid pRL-TK (20 ng) as the internal control, using Lipofectamine® 3000 Reagent (Invitrogen) according to the manufacturer's protocol after culturing in 96-well plates for 12–24 h. In the EZR-AS1 knockdown and EZR-AS1 overexpression experiments, ESCC cells were also transfected with EZR-AS1 siRNA or EZR-AS1 plasmids, respectively. After 48 h, luciferase activity was measured with a Dual-Luciferase Reporter Assay System (Promega) as described (35).

Immunofluorescence

The location of Flag-SMYD3 or truncated SMYD3 in ESCC cells was measured by confocal microscopy as previously described (43,44). Briefly, KYSE 150 cells transfected with Flag-SMYD3 or truncated SMYD3 were fixed with 4% paraformaldehyde for 10 min at room temperature. After washing with PBS, the cells were permeabilized

in 0.1% Triton X-100 in PBS for 10 min at room temperature. After washing with PBS, the cells were blocked for 1 h in PBS containing 5% donkey serum. After washing with PBS, the cells were incubated with anti-Flag (mouse, F3165, Sigma, 1:200 in blocking buffer) for 2 h at room temperature. After washing with PBS, the cells were incubated for 1 h at room temperature with Alexa Fluor® 488-conjugated donkey anti-mouse IgG (H + L) secondary antibodies (715–545–150, 1:200 in PBS, Jackson ImmunoResearch Laboratories, Inc.), followed by washing with PBS. Nuclei were then counterstained with DAPI, and the slides were mounted, and viewed using a confocal microscope (LSM880, Zeiss) with 40×, 1.43 NA, oil-immersion objective lenses.

Cell migration assay

KYSE150 and KYSE510 cells were transfected with two different siRNAs targeting EZR-AS1, or a mixture of siRNAs and EGFP or EZR-EGFP, and then cells were starved in serum-free medium for 12 h after being transfected for 36 h. Cell migration was assessed using an xCELLigence Real-Time Cell Analysis (RTCA) DP instrument (Roche Applied Science, Mannheim, Germany), which was placed in a humidified incubator at 37°C and 5% CO₂. To prepare the CIM plate for the migration assay, each bottom chamber (BC) well was first filled with 170 μ l media, and ensured that a meniscus was formed in each well without trapping a bubble after the well was filled with media. Then the top chamber (TC) was placed facing downwards onto the BC to connect the two chambers, followed by addition of 30 μ l of serum-free media to the top chamber of each well. The CIM plate was placed onto the RTCA DP analyzer inside a 37°C incubator and incubated for 1 h. Cells were trypsinized and resuspended in serum-free media to a concentration of 2×10^5 cells/ml. To each well, 20 000 cells (100 μ l of a 2×10^5 cell/ml suspension) were added in the top chamber before returning the CIM plate into the RTCA DP analyzer inside the 37°C incubator and starting the software (45).

Animal studies

All animal studies were conducted in accordance with protocols approved by the Animal Research Committee of the Shantou Administration Center. Five-week-old male Nude/Nude mice were purchased from Vital River Laboratories (Beijing, China) and maintained in pathogen-free conditions, with water and food *ad libitum*. Mice were randomized into three groups, then footpads were inoculated with 1.0×10^6 cells for each of three stably-transfected KYSE150 cell lines, shRNA-control+GFP (control), shEZR-AS1 + GFP (EZR-AS1 knockdown) and shEZR-AS1 + ezrin-GFP (overexpression of EZR following EZR-AS1 knockdown) (46). Tumor growth was monitored daily, and tumor size was measured (length \times width²) every three 3 days following the appearance of tumors at about 12 days after injection. At approximately 22 days after tumor cell injection, when tumors had spread to the leg, mice were euthanized, and tumors were excised and weighed, then preserved in formalin for histological analysis (46).

RNA-binding protein immunoprecipitation (RIP) assay

We performed UV crosslink experiments as previously described (47). Before the RIP assay, cells in an open dish on ice were placed in a Stratalinker UV-light box and irradiated for 2 min, then collected for RIP assay. RIP assays were performed essentially as described (48–50). Briefly, medium was removed and cold PBS added to each plate. Cells were softly scraped, collected in tubes, and centrifuged at 1000 rpm for 5 min at 4°C. PBS was removed, and cells were lysed in cell lysis buffer (5 mM HEPES [pH 7.4], 85 mM KCl, 0.5% NP40) for 8 min at 4°C with shaking. Samples were transferred to tubes and centrifuged at 5000 rpm for 5 min at 4°C. Supernatant was removed, nuclei lysis buffer (20 mM Tris-HCl [pH 8.0], 200 mM NaCl, 1 mM EDTA [pH 8.0], 1 mM EGTA [pH 8.0], 0.1% SDS, 1% NP-40, 1 × proteinase inhibitor cocktail and 1% RNase inhibitor) was added, and then the tubes were placed on a wheel for 30 min at 4°C. Then nuclear lysates were sonicated and 10% of the lysate extracted with TRIzol (Invitrogen) to serve as ‘input’. The remainder of the lysate was incubated with 40 μl protein G-coupled Dynabeads (Life Technologies) for 30 min at 4°C to decrease the background, followed by washing in lysis buffer and adding protein G-coupled Dynabeads with 3 μg anti-SMYD3 antibody, anti-RNA Pol II antibody, anti-SP1 antibody or IgG control, then rotated overnight at 4°C. After beads were sequentially washed 4 times in IP buffer (1:1 of nuclei lysis buffer without SDS) and two times in IP buffer containing 400 mM KCl. RNA was isolated by TRIzol (Invitrogen), incubated with DNase I (Sigma) and subjected to qRT-PCR. All RIP assays were performed in triplicate (primers in Table 1).

RNA pull-down assay

RNA pull-down assays were performed essentially as previously described (48–50). Briefly, equal amounts of EZR-AS1, EZR-AS1 antisense, EZR-AS1/1–131, EZR-AS1/1–281, EZR-AS1/131–281 and EZR-AS1/131–362 plasmids were linearized at the *Hind* III site and purified from the enzyme and buffer by phenol/chloroform extraction and ethanol precipitation. Then plasmids were *in vitro*-transcribed with a Biotin RNA Labeling Mix (Roche) and T7 RNA polymerase (Roche) to label transcripts with biotin. Biotin-labeled RNA was treated with RNase-free DNase I (Roche), and purified with an RNeasy Mini Kit (Qiagen, Valencia, CA). The efficiency of transcribed biotinylated EZR-AS1 RNA and antisense EZR-AS1 RNA *in vitro* was detected by a Chemiluminescent Nucleic Acid Detection Module (Thermo, No. 89880), and then an equal amount of biotin-labeled RNA or unrelated RNA was added as a control to streptavidin Dynabeads. Samples were incubated on a turning wheel at room temperature for 15 min to immobilize RNA on the streptavidin dynabeads, then supernatant was removed and beads were washed with wash buffer (10 mM Tris-HCl, [pH 7.5], 1 mM EDTA, 2 M NaCl and 0.1% Tween-20). At the same time, nuclear lysates were prepared using nuclei lysis buffer (300 mM NaCl, 20 mM Tris-HCl [pH 8.0], 0.2% Tween-20, 1 mM EDTA) as described in the RIP assay. Nuclear lysates were added to beads with immobilized RNA, and then incubated

on a turning wheel overnight at 4°C. After stringent washing with nuclei lysis buffer, samples were boiled for 10 min at 100°C in loading buffer, and target proteins detected by standard western blotting.

Chromatin immunoprecipitation (ChIP)

Cells were grown to 60–70% confluence in 10-cm plates, and then ChIP was performed using an EZ-Magna ChIP Chromatin Immunoprecipitation Kit (Millipore). In short, cells were crosslinked with 1% formaldehyde for 10 min at room temperature, followed by the addition of glycine to each dish to quench unreacted formaldehyde. Then, after two washes with ice cold PBS, cells were lysed with cell lysis buffer and centrifuged at 800 × *g* at 4°C for 5 min in a microcentrifuge. Supernatant was carefully removed and nuclear pellets were re-suspended in 0.5 ml of nuclear lysis buffer, then sonicated to create appropriately sized chromatin fragments. After sonication, the sonicated nuclei were centrifuged to remove insoluble material. Subsequently, supernatant was transferred to clean microfuge tubes in 50 μl aliquots, which was sufficient for one immunoprecipitation. Then 3 μg anti-SMYD3 antibody, anti-RNA polymerase II antibody, anti-H3K4me3 antibody or normal IgG was added to each nuclear extract, and extracts were further incubated at 4°C overnight. Nuclear extracts were then incubated with magnetic protein A/G beads for 2 h at 4°C to capture protein/DNA complexes, then beads were sequentially washed with low salt buffer, high salt buffer, LiCl wash buffer and TE buffer, then protein/DNA complexes were eluted and reverse cross-linked to free the DNA. Purified DNA was analyzed by qPCR with SYBR Green Master Mix (Promega), and relative enrichment was normalized to input, and expressed relative to values obtained after normal IgG immunoprecipitation. Primers used are listed in Table 1.

For the RNase ChIP assay, KYSE150 cells were permeabilized in PBT (PBS; 0.05% Tween 20) and treated with RNase as previously described (42). Upon completion of RNase treatment, a ChIP assay was performed, as described above.

Statistical analysis

Statistical analysis was performed using SPSS 18.0 software. Results are presented as mean ± SD. Student’s *t*-tests were used to compare data between groups. Statistical significance was considered at $P < 0.05$.

RESULTS

EZR-AS1 upregulates EZR expression in ESCC

As an antisense lncRNA of the EZR gene, we investigated the possible relationship between EZR-AS1 and EZR, initially by examining their transcription levels in 15 pairs of human ESCC tissues and pair-matched normal esophageal tissues by RNA-sequencing (<http://www.ncbi.nlm.nih.gov/sra/>, accession number SRP064894). The data revealed a positive correlation between EZR-AS1 and EZR gene expression ($r = 0.861$) in ESCC tissue (Figure 1B). Further, the expression of EZR-AS1 and EZR in a panel of seven

human esophageal squamous cell carcinoma cell lines, and an additional 30 cases of human ESCC tissues displayed this positive correlation, as well as lower expression of EZR-AS1 compared to EZR, consistent with the RNA-seq data (Figure 1C). In addition, both EZR-AS1 and EZR were expressed at higher levels in ESCC tissue compared to normal tissue, but the correlation coefficient (r), of 0.527, was low in 30 cases of pair-matched normal esophageal tissues (Supplementary Figure S2). These results suggest that antisense lncRNA EZR-AS1 could modulate EZR gene expression in ESCC cells. To confirm this hypothesis, we silenced EZR-AS1 expression by two different siRNAs that targeted EZR-AS1 in regions that did not overlap with EZR mRNA sequences. Compared with control, when the level of EZR-AS1 was decreased by 80%, the expression of EZR (variant 1), both at the mRNA and protein levels, was also reduced in both KYSE150 and KYSE510 cells (Figure 1D and F). The same result was observed in KYSE150 cells with stably silenced EZR-AS1 expression (Figure 1E and G). Furthermore, the overexpression of EZR-AS1 accompanied the enhanced expression of EZR (variant 1), both at the mRNA and protein levels, in KYSE150 cells (Figure 1H and I). However, the expression of EZR (variant 2) was unaffected following either silencing or overexpression of EZR-AS1 (Figure 1D, E and H). In addition, to ensure that EZR was reduced at the RNA level upon down-regulation of EZR-AS1, we characterized EZR levels by using another primer for the exon 12 of EZR gene variant 1 (EZR-exon 12-F/R, Table 1). As expected, EZR expression was significantly decreased following knockdown of EZR-AS1 and increased by the overexpression of EZR-AS1 (Supplementary Figure S3). Taken together, these results indicate that EZR-AS1 up-regulates EZR expression at both the RNA and protein levels in ESCC.

EZR-AS1 up-regulates EZR expression to promote ESCC cell migration both *in vitro* and *in vivo*

To explore the mechanism by which EZR-AS1 enhances EZR expression in ESCC, we used siRNA-mediated knockdown to exogenously manipulate expression of EZR-AS1. Real-time cell analysis (RTCA) showed that knockdown of EZR-AS1 did not affect cell proliferation compared with the control cells (Supplementary Figure S4), but cell migration was significantly repressed (Figure 2A). Transwell migration assays supported the same conclusions (Supplementary Figure S5A). RTCA of KYSE150 cells, stably transfected with shEZR-AS1 to stably silence EZR-AS1 expression, showed that knockdown of EZR-AS1 expression significantly reduced ESCC cell migration compared with the control cells (Figure 2B). Rescue of EZR expression in the RTCA assay showed that, though the migration was still less than the control, overexpression of EZR could significantly reverse EZR-AS1 knockdown-mediated suppression of ESCC cell migration (Figure 2C and D), similar to data from the transwell assay (Supplementary Figure S5B), further confirming the role of EZR-AS1 in cell migration. These results suggest that EZR-AS1 up-regulates EZR expression to promote cell migration.

Further to explore whether the regulation of EZR by EZR-AS1 affects ESCC tumorigenicity *in vivo*, KYSE150

cell lines were stably transfected with shRNA-control+GFP (control), shEZR-AS1+GFP (EZR-AS1 knockdown) or shEZR-AS1+ezrin-GFP (overexpression of EZR following EZR-AS1 knockdown), and then were inoculated directly into the footpads of nude mice. More than twenty days after the injection, silencing of EZR-AS1 decreased the tumor volume compared with the control group. The mean tumor weight and the extent of invasion, in the shEZR-AS1 group, were lower compared with the control group (Figure 3A–E and Supplementary Figure S6), and the number of metastatic nodules was reduced in the shEZR-AS1 group (Figure 3E). Moreover, overexpression of EZR reversed the EZR-AS1 knockdown-mediated reduction of tumor volume, tumor weight, and number of metastatic lymph nodules (Figure 3A–E and Supplementary Figure S6). These results indicate that EZR-AS1 promotes ESCC cell migration *in vivo* through elevation of EZR expression.

EZR-AS1 regulates EZR transcriptional activity in ESCC cells by interacting with RNA polymerase II, but not by affecting the binding of SP1 and AP-1 transcription factors

Since the intracellular localization of antisense lncRNAs corresponds to the molecular mechanisms by which lncRNAs regulate genes, from transcriptional activation to post-translational protein modification (51,52), we performed subcellular fractionation to identify the location of EZR-AS1 in ESCC cells. EZR-AS1 expression was 4-fold more abundant in the nuclear fraction relative to the cytoplasm in ESCC cells (Figure 4A), suggesting that EZR-AS1 may modulate EZR transcriptional expression. Further, to identify whether there was an EZR-AS1 responsive region, we transiently co-transfected three luciferase reporter constructs containing different fragments of the EZR promoter (i.e. the full-length cloned fragment (–1324/+134), a truncated cloned fragment (–697/+134) or an EZR promoter fragment (–87/+134) with NC or siEZR-AS1 into ESCC cells. Luciferase reporter gene assays showed that knockdown of EZR-AS1 significantly reduced the –1324/+134 luciferase activity. Notably, the activity of the –87/+134 construct was significantly decreased following knockdown of EZR-AS1 (Figure 4B), whereas overexpression of EZR-AS1 enhanced the activity of the –87/+134 construct (Figure 4C). The activity of pGL3-promoter and –1324/–697, which were used as negative controls, were not affected by EZR-AS1 knockdown or overexpression (Figure 4D). These results indicate that EZR promoter region –87/+134 contained the EZR-AS1 responsive sites and was activated by EZR-AS1.

Based on our previous demonstration that SP1/AP-1 binding sites, located within the EZR promoter region (–87/+134), not only function as basal transcriptional elements, but also serve as a composite TPA-responsive element (TRE) (35,37), we speculated that EZR-AS1 may recruit SP1 and AP-1 transcription factors to up-regulate EZR expression. However, luciferase reporter gene assays revealed that upon silencing of EZR-AS1 expression, SP1 and c-Jun continued to enhance the activity of –87/+134 construct, indicating that EZR-AS1 up-regulates EZR transcriptional expression, but did not affect the binding of SP1 and AP-1 transcription factors (Figure 4E).

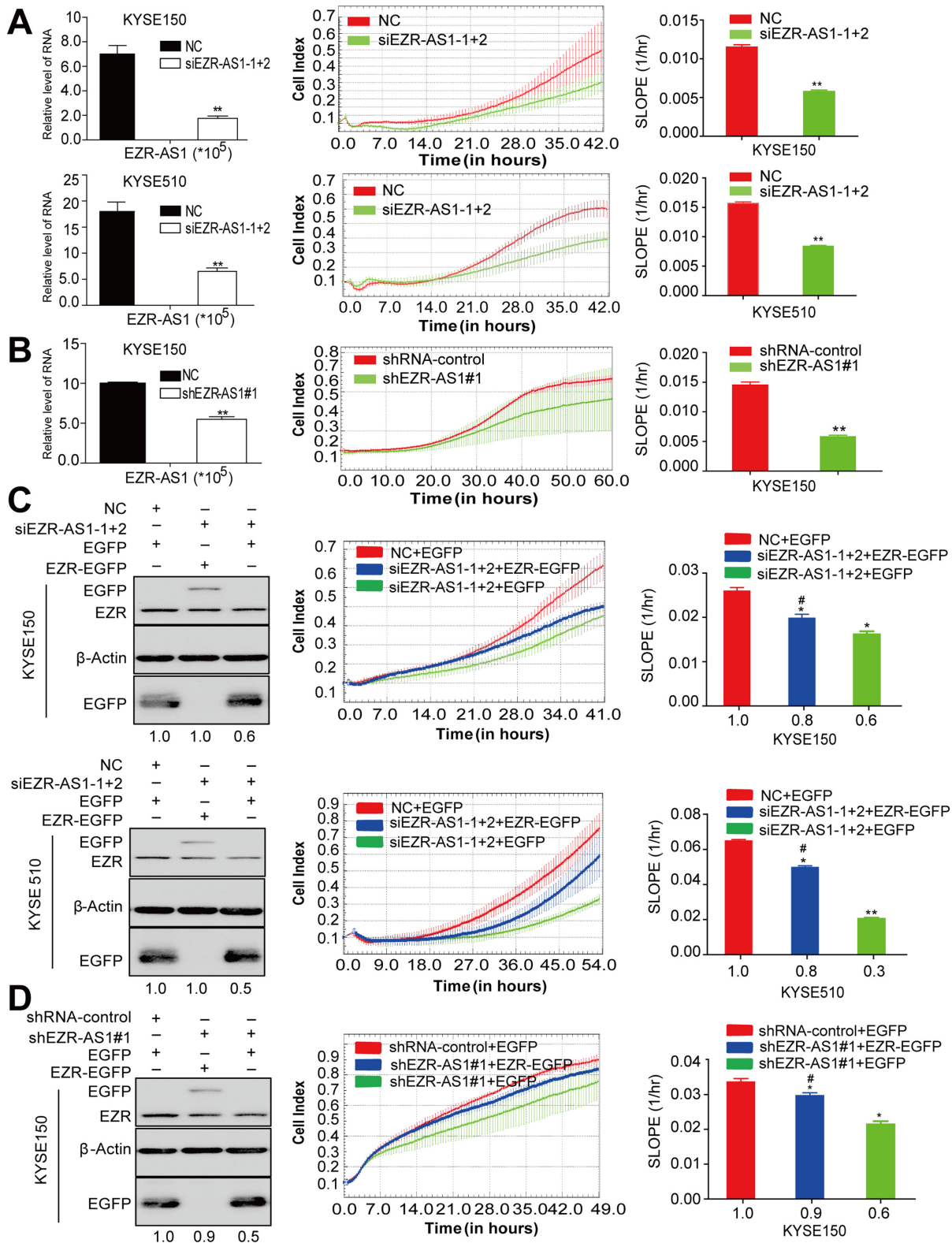


Figure 2. EZR-AS1 increases EZR expression to promote ESCC cell migration. (A) KYSE150 and KYSE510 cells were transfected with siRNAs against EZR-AS1, and cell migration was measured by a real-time cell analyzer (RTCA) DP (dual plate) instrument. (B) Cell migration of stable EZR-AS1-knockdown KYSE150 cells. qRT-PCR assay detected EZR-AS1 expression in (A) and (B) cells. Data represent the mean \pm SD ($n = 3$). Graphs in (A) and (B) represent data from three independent transfection experiments. (C) Cell migration of KYSE150 and KYSE510 cells over-expressing EZR following EZR-AS1 silencing by two different siRNAs. (D) Effect of EZR overexpression on the cell migration in EZR-AS1-knockdown KYSE150 cells. Mean \pm SD ($n = 3$). Graphs represent data from three independent transfection experiments in (A) to (C). * $P < 0.05$ or ** $P < 0.01$, compared with the NC group; # $P < 0.05$, compared with the siEZR-AS1 or shEZR-AS1 group.

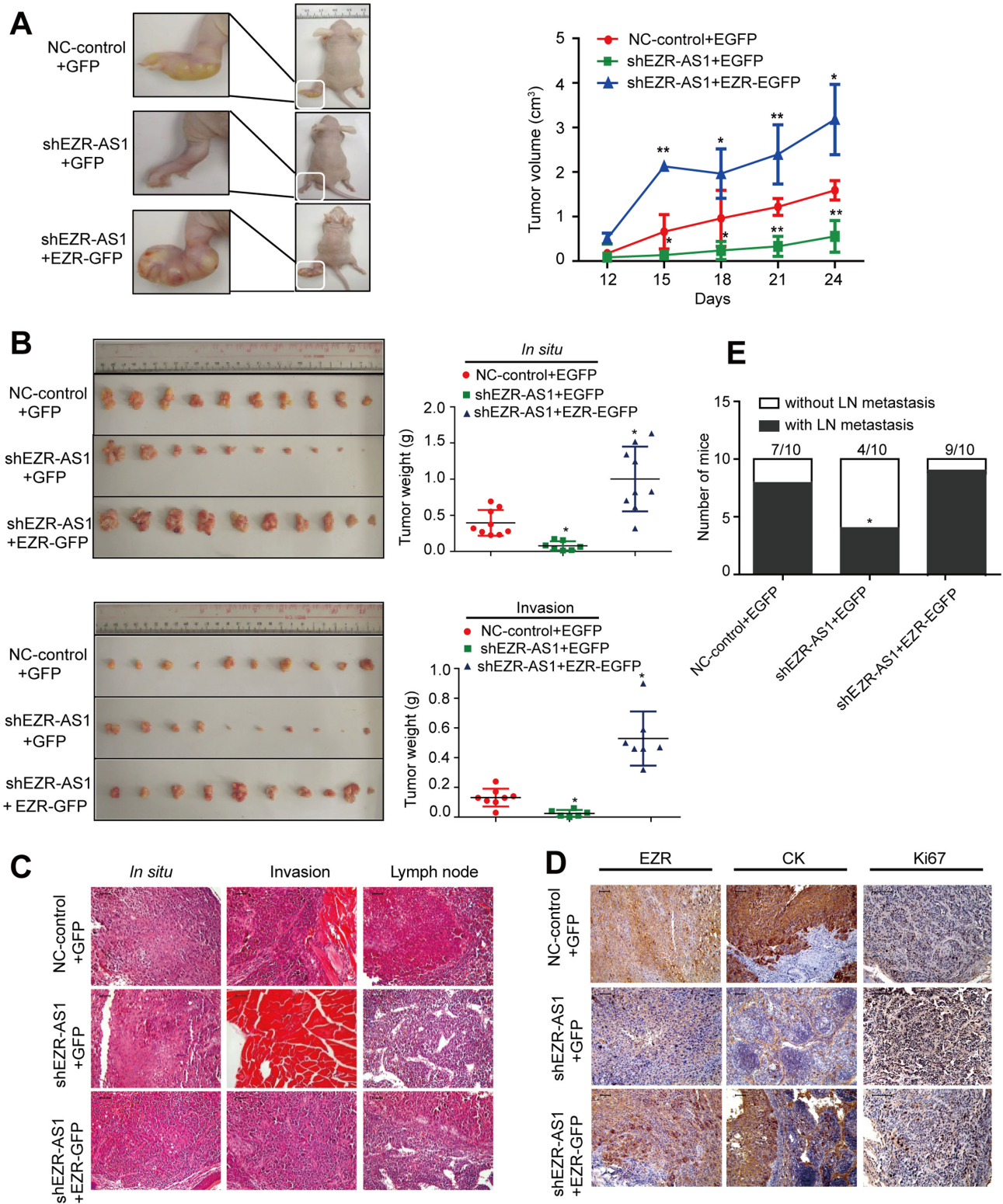


Figure 3. EZR-AS1 up-regulates EZR expression and promotes tumor cell invasion and migration. (A) Tumor volume, *left*, representative images of tumor volumes 22 days after footpad injection with the indicated cells; *right*, tumor volume in each group over time following footpad injection with the indicated cells. (B) Representative images of primary tumor weight (*upper*) and invaded tumor weight from (A) over time (*below*). Data are shown as mean \pm SD ($n = 10$), * $P < 0.05$ or ** $P < 0.01$. (C) Hematoxylin and eosin-stained (H&E) images of primary tumors, invaded tumors and lymph nodes from mice in (A). (D) Immunohistochemistry analysis for EZR, CK (cytokeratin, a marker of squamous epithelial cells) and Ki67 in tumor tissue from mice in (A). The shRNA-control+GFP (control), shEZR-AS1 + GFP (EZR-AS1 knockdown) and shEZR-AS1+ezrin-GFP (overexpression of EZR after EZR-AS1 knockdown) cells following injection of 1×10^6 cells into the footpads of mice (ten mice per group), respectively. (E) Number of mice with lymph node metastases.

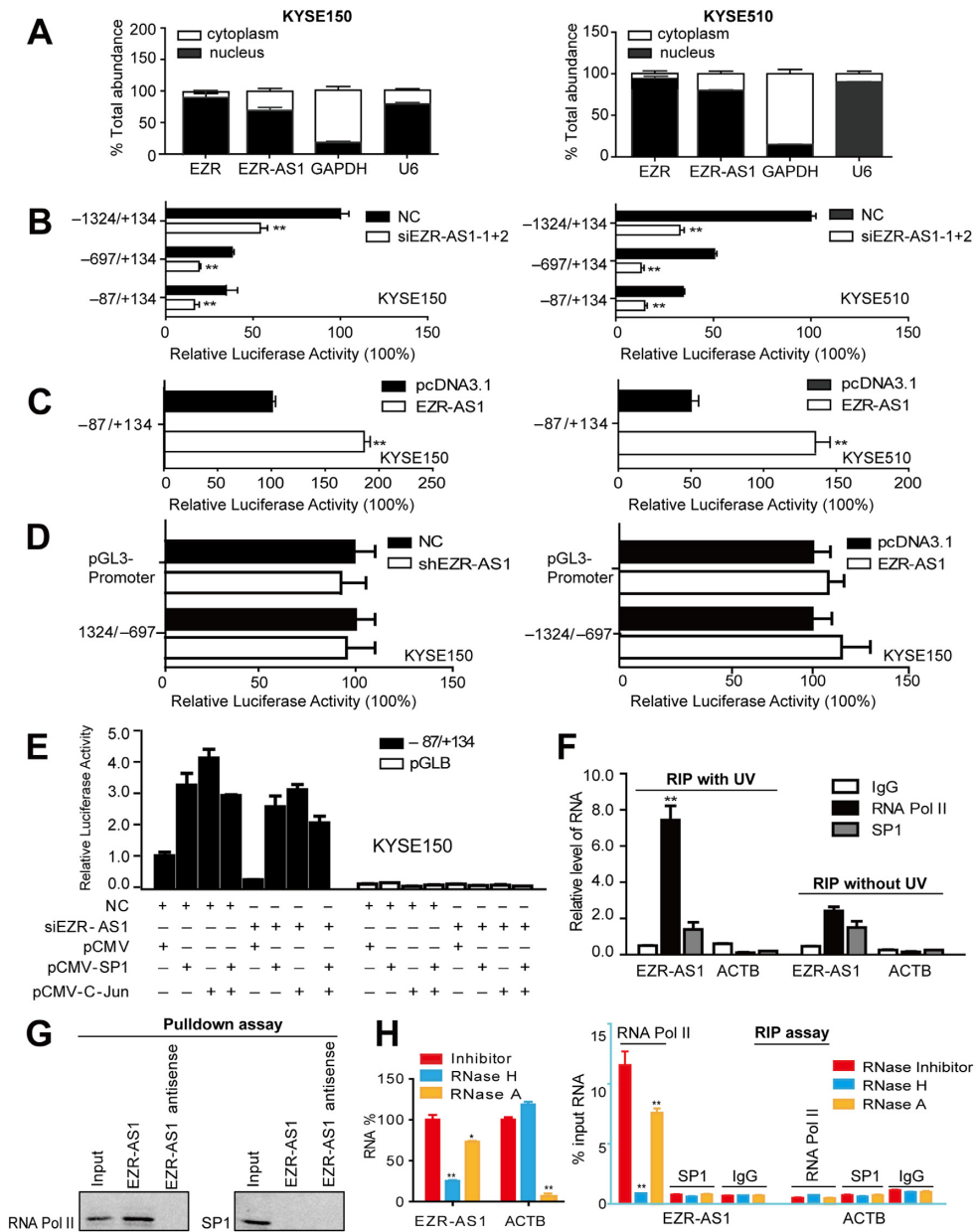


Figure 4. EZR-AS1 regulates transcription of EZR through an interaction with RNA polymerase II. (A) Relative expression of EZR-AS1 and EZR in nuclear RNA and cytoplasmic RNA was detected by qRT-PCR in KYSE150 and KYSE510 cells. GAPDH and U6 were used as the cytoplasmic and nuclear loading controls, respectively. (B) Luciferase reporter genes driven by the -1324/+134, -697/+134 or -87/+134 EZR promoter region were transiently co-transfected with NC or siEZR-AS1-1+2 into KYSE150 and KYSE510 cells, and luciferase activity was measured after 48 h. *Firefly* luciferase activity was normalized to *Renilla* luciferase activity, and the relative value from the ESCC cells co-transfected with both pGLB-hE (-1324/+134) and NC was set to 100%. (C) pGLB-hE (-87/+134) was transiently co-transfected with pcDNA3.1 or EZR-AS1 into KYSE150 and KYSE510 cells, and reporter gene activity was measured by dual-luciferase analysis after transfection for 48 h. *Firefly* luciferase activity was normalized to *Renilla* luciferase activity and the relative value from the ESCC cells co-transfected with both pGLB-hE (-87/+134) and pcDNA3.1 was set to 100%. (D) pGL3-promoter and pGLB-hE (-1324/-697) were used as the negative control in EZR-AS1 stably-silenced or overexpressing KYSE150 cells. The detailed experimental procedure is the same as described above in (B) and (C). (E) pGLB or pGLB-hE (-87/+134), and pCMV, pCMV-SP1 or pCMV-c-Jun constructs were transiently co-transfected with NC or siEZR-AS1-1+2 into KYSE510 cells. After 48 h, luciferase activity was measured. *Renilla* luciferase activity served as the internal control and the relative value from ESCC cells co-transfected with pGLB, pCMV and NC was set to 1. (F) RNA immunoprecipitation (RIP) assay. In the RNA immunoprecipitation with UV, KYSE150 cells were UV-crosslinked. Then RNA immunoprecipitation was used to detect endogenous EZR-AS1 levels bound to RNA Pol II in UV-crosslinked cells or non-crosslinked cells. IgG, and SP1 antibody was used as negative controls. (G) RNA pull-down of biotin-labeled EZR-AS1 in KYSE150 cells. Western blot detected RNA polymerase II (RNA Pol II) in immunoprecipitates. Biotin-labeled EZR-AS1 antisense followed by probing for SP1 in precipitates was used as the negative control. (H) RIP assay after treatment with RNase H or RNase A. *left*, qRT-PCR analysis of endogenous EZR-AS1 levels in KYSE150 cells following permeabilization and treatment with RNase H or RNase A. Relative values for EZR-AS1 levels were normalized to the corresponding values for the RNase inhibitor-treated cells. *right*, UV-crosslinked KYSE150 cells were treated with RNase H or RNase A and then RIP was performed using anti-RNA Pol II and -SP1 antibody, or control IgG. Total RNA was isolated and detected by qRT-PCR. ACTB (β -actin) was used as the negative control. Mean \pm SD ($n = 3$). All graphs show data from three independent experiments in (A) to (H). * $P < 0.05$ or ** $P < 0.01$.

To explain why EZR-AS1 promotes the activity of EZR promoter $-87/+134$, independent of SP1 and AP-1 transcription factors, we performed RIP and RNA pull-down assay. The results showed a strong enrichment of EZR-AS1 by immunoprecipitation for RNA polymerase II, compared to immunoprecipitation for SP1 or IgG control in both UV-crosslinked and non-crosslinked cells. Moreover, the signal in the UV-crosslinked cells was stronger than that in the non-crosslinked cells (Figure 4F). In the RNA pull-down experiment, we firstly prepared biotin-labeled EZR-AS1 RNA and biotin-labeled EZR-AS1 antisense RNA, detected the amount of biotin-labeled RNA under the same volume (Supplementary Figure S7), and then performed an RNA pull-down assay. A clear band, corresponding to RNA polymerase II protein, was observed in both the input and EZR-AS1 fraction, whereas no band was observed in the EZR-AS1 antisense fraction (Figure 4G). Moreover, EZR-AS1 RNA did not pull down SP1, and EZR-AS1 antisense RNA did not pull down RNA polymerase II (Figure 4F and G). These results indicate that an interaction exists between EZR-AS1 and RNA polymerase II. This interaction possibly occurs within EZR promoter region, since RNA polymerase II is highly enriched at the promoters of genes with active transcriptions. To further confirm this interaction, EZR-AS1 RNA abundance was reduced by first treating cells with RNase H or RNase A (Figure 4H, *left*), and then performing a RIP assay. The results showed that the interaction between EZR-AS1 and RNA polymerase II was markedly reduced, and was accompanied by the degradation of endogenous EZR-AS1, compared with the RNase inhibitor conditions (Figure 4H, *right*). To sum up, these data demonstrate that EZR-AS1 forms a complex through an interaction with RNA polymerase II to activate the transcription of EZR. Given the function of RNA polymerase II in activating gene promoters, these results indicate that EZR-AS1 and RNA polymerase II might enhance the promoter activity of EZR.

EZR-AS1 enhances EZR expression by causing SMYD3 redistribution and binding of SMYD3 at a site within the GC-rich region downstream of the EZR promoter

Previous reports demonstrate that antisense transcripts participate in epigenetic gene regulation through providing a scaffold for recruitment of histone-modifying enzymes (42,53–55). We speculate that there may be other molecules involved in EZR-AS1-mediated regulation of EZR expression in addition to EZR-AS1 involvement as a member of RNA pol II complex. It has been reported that SMYD3, a histone H3-lysine 4 (H3-K4)-specific methyltransferase, binds to a 5'-CCCTCC-3' motif present in the promoter region of downstream genes to transactivate the genes (56,57). We previously found that SMYD3 up-regulates EZR transcription in ESCC cells (39). Therefore, we predicted that EZR-AS1, as a member of the RNA polymerase II complex, could recruit SMYD3 to the EZR gene. To test this prediction, we firstly knocked down SMYD3 using SMYD3 shRNA reported previously (39), and confirmed that endogenous EZR expression was reduced, at both the mRNA and protein levels, by at least 50% compared with the control group (Figure 5A, B and Supplementary Figure S8).

However, there was no effect on the expression of EZR-AS1 (Supplementary Figure S8). Then we designed four pairs of chromatin immunoprecipitation primers targeting the SMYD3 binding site (SBS), in addition to several control primers targeting genomic locations that are not expected to be bound by SMYD3 on the EZR gene, and performed a ChIP assay (Figure 5C, *above*). Results showed that SMYD3 bound to the SBSs, but did not bind to 1792/1578 (exon 12 of EZR), 140/24 (EZR promoter) or $-804/-885$ (5'flanking fragment), which do not have SMYD3 binding sites, in the EZR gene (Figure 5C, *below*). In addition, knockdown of SMYD3 decreased the enrichment of SMYD3 protein from SBS-1 to SBS-4 (Figure 5D). These results suggest that SMYD3 binds to the specific region, containing SMYD3 binding sites, to up-regulate EZR expression, consistent with our previous results (39).

Next, to evaluate the role of EZR-AS1 in SMYD3-mediated EZR expression, we knocked down or overexpressed EZR-AS1, and then performed ChIP assays. Results showed a decrease SMYD3 occupancy at SBS-1 and SBS-2 accompanied EZR-AS1 silencing, and conversely showed increased the binding of SMYD3 at SBS-1 and SBS-2 after overexpression of EZR-AS1, whereas there was inconsistent and/or no clear difference in SMYD3 occupancy at SBS-3 and SBS-4 (Figure 5E and F). These results suggest that EZR-AS1 caused accumulation of SMYD3 at SBS-1 and SBS-2, and was involved in SMYD3-mediated EZR expression.

Analysis of the EZR gene, using the CpGPlot Program (www.ebi.ac.uk/emboss/cpgplot) (58), showed that both SBS-1 and SBS-2 were located in the GC-rich region of the EZR promoter (Figure 1A). Compared with typical promoters, GC-rich promoters are not conducive to gene transcription (59). Considering SMYD3 is a histone H3-lysine 4 (H3-K4)-specific methyltransferase (56,57), we surmised that EZR-AS1-induced SMYD3 redistribution may contribute to chromatin remodeling. To prove this, changes in H3K4me3 were detected. ChIP assay showed a similar decrease of H3K4me3 occupancy, at SBS-1 and SBS-2, accompanying EZR-AS1 silencing, and increased H3K4me3 content at SBS-1 and SBS-2 following overexpression of EZR-AS1 (Figure 5E and F). Thus, these results suggest that the accumulation of SMYD3 at SBS-1 and SBS-2, caused by EZR-AS1, is conducive to chromatin remodeling to enhance EZR transcription.

To further investigate which SMYD3 binding site was the key site for promotion of EZR transcription, we constructed a serious luciferase reporter gene plasmids, driven by various regions of the EZR promoter (Figure 5G, *left*), and then performed luciferase reporter gene assays. Compared with the empty vector control, the activity of both pGLB-hE ($-1324/+550$) and pGLB-hE ($-87/+550$) promoters was more than 2-fold increased by overexpression of EZR-AS1, and the activity was reduced by $\sim 50\%$ upon silencing of EZR-AS1 (Figure 5G, *right*, Supplementary Figure S9). However, when the SBS-1 was mutated, overexpression of EZR-AS1 could not increase reporter gene activity; and mutation of SBS-2 had no effect on the increased activity following EZR-AS1 overexpression (Figure 5G, *right*). To confirm the involvement of SBS-1 in EZR-AS1-mediated enhancement of transcription, we con-

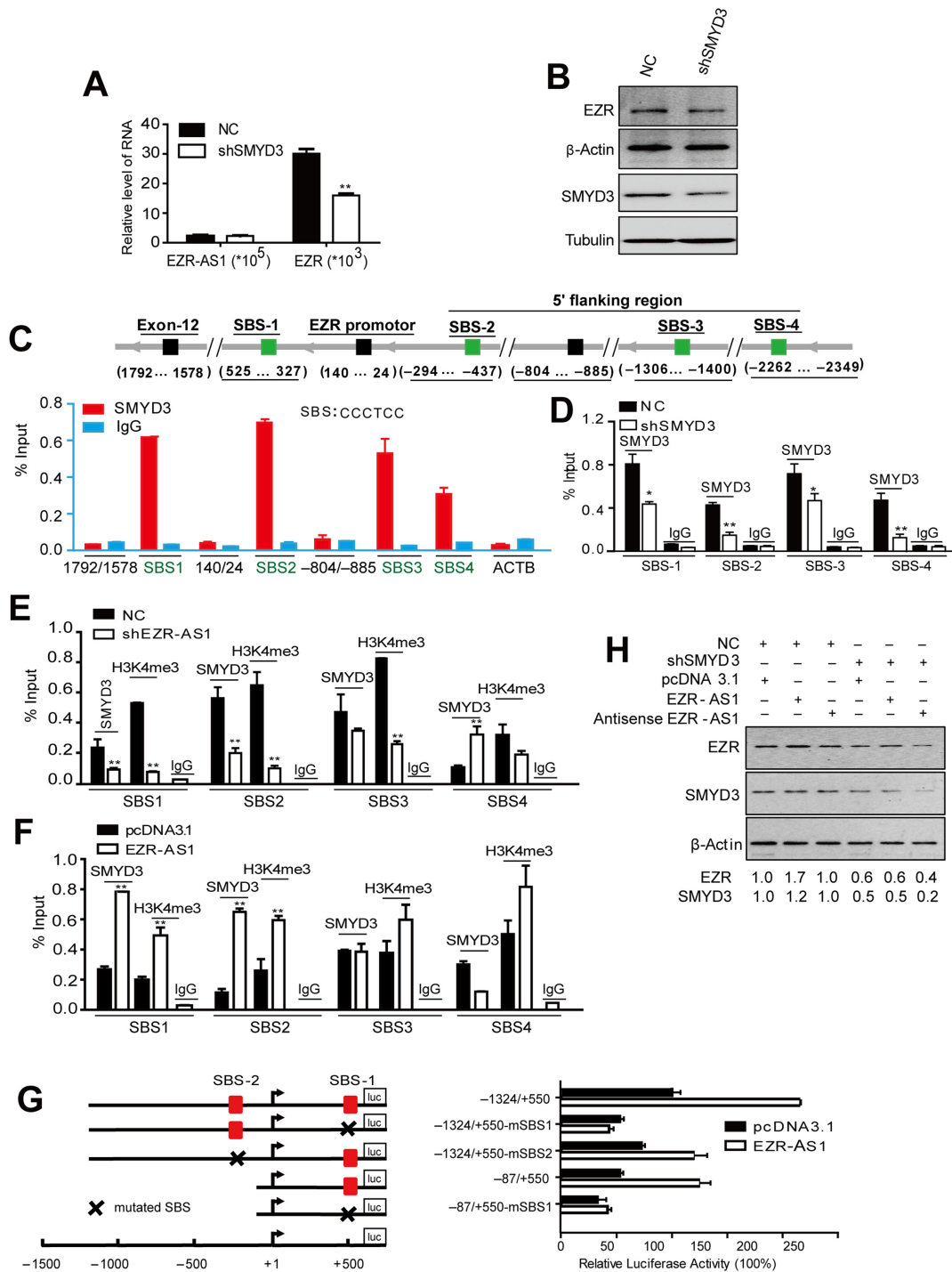


Figure 5. EZR-AS1 is involved in the SMYD3-mediated EZR expression. (A) Total RNA was prepared from KYSE150 cells following knockdown of SMYD3 by lentiviral transduction of two different shRNAs, and the level of EZR-AS1 and EZR were measured by qRT-PCR. (B) Western blot analysis with antibodies against EZR or SMYD3 in KYSE150 cells from (B). β-Actin was the loading control. (C) Schematic representation of predicted SMYD3 binding sites and the location of control primers for chromatin immunoprecipitation within the EZR gene and its flanking region (*above*). ChIP assay in KYSE150 cells, using anti-SMYD3 antibody, followed by qPCR to quantify the amount of genomic EZR DNA (*below*). ACTB was the negative control. (D) ChIP assay in SMYD3-knockdown KYSE150 cells, using an anti-SMYD3 antibody. The association between SMYD3 and SMYD3 binding sites in the EZR promoter region was measured by qPCR. (E) ChIP-qPCR assay of the EZR promoter region using anti-SMYD3 or anti-H3K4me3 antibody in EZR-AS1-knockdown KYSE150 cells. (F) ChIP-qPCR assay of the EZR promoter region using anti-SMYD3 or anti-H3K4me3 antibody in EZR-AS1 over-expressing KYSE150 cells. (G) Luciferase reporter gene constructs (*left*) were transiently co-transfected with pcDNA3.1 or EZR-AS1 into KYSE150 cells, and reporter gene activity was measured after 48 h by dual-luciferase analysis (*right*). Firefly luciferase activity was normalized to Renilla luciferase activity and the relative value from the ESCC cells co-transfected with both pGLB-hE (-1324/+550) and pcDNA3.1 was set to 100%. (H) Western blot analysis of EZR in SMYD3-knockdown KYSE150 cells overexpressing EZR-AS1. Data are from three independent experiments in (A)–(H). Mean ± SD (*n* = 3). **P* < 0.05 or ***P* < 0.01.

structed EZR promoter plasmids with SBS-2, but without SBS-1, and then performed luciferase reporter gene assays (Supplementary Figure S10). Whether SBS-2 was mutated or not, all reporter activity was decreased by about 50% after silencing EZR-AS1 and increased by more than 50% after overexpression of EZR-AS1 (Supplementary Figure S10). These indicated that the SBS-1 was the key binding site involved in the up-regulation of EZR transcription induced by EZR-AS1. Furthermore, western blot assays showed that overexpression of EZR-AS1 lost the ability to upregulate EZR expression in SMYD3 knockdown cells (Figure 5H). These results suggest that EZR-AS1, as a member of the RNA pol II complex, recruits SMYD3 to SBS-1 within the GC-rich stretch downstream of the EZR promoter, causing binding of SMYD3 and methylation of H3K4, resulting in the up-regulation of EZR transcription in ESCC cells.

EZR-AS1 interacts with SMYD3 to promote SMYD3 binding to the EZR gene

To explore how EZR-AS1 recruits SMYD3 to the EZR promoter, we further investigated an interaction between EZR-AS1 and SMYD3, in both UV-crosslinked and non-crosslinked cells, by RIP assay. Endogenous EZR-AS1 was enriched in the anti-SMYD3 RIP fraction compared to the non-specific IgG fraction in both UV-crosslinked and non-crosslinked cells. Moreover, compared to non-crosslinked cells, UV-crosslinked cells showed better signal strength (Figure 6A). Similarly, RNA pull-down showed a clear band, corresponding to SMYD3 protein, in both the input and EZR-AS1 fraction, whereas no band was observed in the EZR-AS1 antisense fraction (Figure 6B). Therefore, the data demonstrate that EZR-AS1 interacts with SMYD3 specifically and directly.

To identify the functional domain within EZR-AS1 responsible for associating with SMYD3, we cloned a series of deletion constructs of EZR-AS1, and then performed an RNA pull-down assay. As shown in Figure 6C, only full-length EZR-AS1 interacted with SMYD3, whereas the truncated lncRNAs could not, suggesting that the interaction between EZR-AS1 and SMYD3 protein involves a novel mechanism that depends on the tertiary structure of the full length of EZR-AS1, rather than the function of one or more EZR-AS1 domains.

We also cloned a series of Flag-tagged SMYD3 deletion constructs to identify its EZR-AS1-binding domain. We employed western blotting and immunofluorescence to confirm that the truncated plasmid was correctly expressed and positioned in the nucleus (Figure 6D and E), and then a RIP assay was performed. Results demonstrate that only the full-length SMYD3 protein associated with EZR-AS1 (Figure 6D), similar to the results with EZR-AS1. Collectively, these results show that the EZR-AS1 interact with SMYD3 to cause SMYD3 binding to SBS-1, within the GC-rich region downstream of the EZR promoter, resulting in the up-regulation of EZR transcription.

To further confirm the relationship of EZR-AS1 with both SMYD3 and RNA polymerase II in the regulation of EZR transcription, we reduced EZR-AS1 RNA levels by treatment with RNase H or RNase A (Figure 4H, *left*), and

then performed a ChIP assay. Results showed there was a total release of SMYD3 from SBS-1, accompanied by the degradation of endogenous EZR-AS1, whereas RNA polymerase II remained bound to EZR SBS-1 (Figure 6F), suggesting that EZR-AS1 only recruits SMYD3, but not RNA polymerase II, to the EZR promoter to regulate EZR transcription.

DISCUSSION

Altogether, our work demonstrates that antisense lncRNA EZR-AS1 complexes with RNA polymerase II to activate the transcription of EZR. EZR-AS1 recruits SMYD3 to SMYD3 binding sites present in the GC-rich region downstream of the EZR promoter, causing local accumulation of SMYD3 and concomitant trimethylation of H3K4 at the EZR gene. Finally, the interaction of EZR-AS1 with SMYD3 further enhances EZR transcription and expression to increase migration of ESCC cells (Figure 7).

RNA-seq data from 15 ESCC samples confirmed the expression of EZR-AS1 in ESCC and suggested a positive correlation between EZR-AS1 and EZR expression, consistent with the qRT-PCR results from ESCC cells and an additional 30 cases of ESCC samples (Figure 1B and C). Similar to the ability of lncRNA ANRASSF1 to regulate RASSF1A expression and promote cell motility (42), our work, both *in vivo* and *in vitro*, demonstrates that EZR-AS1 up-regulates EZR expression and enhances ESCC cell migration, suggesting that EZR-AS1 may be a potential therapeutic target for ESCC clinical therapy.

Just as BDNF-AS (60), ZEB2-AS (61) and BACE1-AS (62,63) affect target gene expression, we show that EZR-AS1 up-regulates EZR expression (Figure 1D–I). However, unlike other lncRNAs, EZR-AS1 does not influence transcription factor binding to the transcription region (Figure 4E), but rather forms a complex with RNA polymerase II to activate the transcription of EZR (Figure 4F–H). Rescue experiments show that overexpression of EZR does not lead to a complete rescue of the cell motility inhibited by EZR-AS1 silencing, which suggests that EZR-AS1 not only regulates EZR expression, but also affects other target genes as well (Figure 2C and D). This is consistent with other mechanisms found for antisense lncRNA-mediated regulation (64). When antisense lncRNA triggers DNA or chromatin modification, expansion of the modification may affect nearby promoters or enhancers, or may regulate a cluster of genes, an example being the Kcnq1 imprinted locus (64).

The functions and mechanisms of antisense RNAs are diverse, from transcription to translation (51,52), with antisense RNAs acting as decoys or scaffolds to recruit chromatin-associated proteins in order to regulate gene expression (53,55,65). In this study, ChIP assays show that silencing EZR-AS1 decreases SMYD3 binding on the EZR gene (Figure 5E). In contrast, overexpression of EZR-AS1 leads to complete rescue of the SMYD3 occupancy (Figure 5F). In addition, we show that EZR-AS1 does not up-regulate EZR expression following SMYD3 knockdown (Figure 5H), and that the interaction between EZR-AS1 and SMYD3 depends on the full length of EZR-AS1 (Figure 6C), not the small regions comprising individual func-

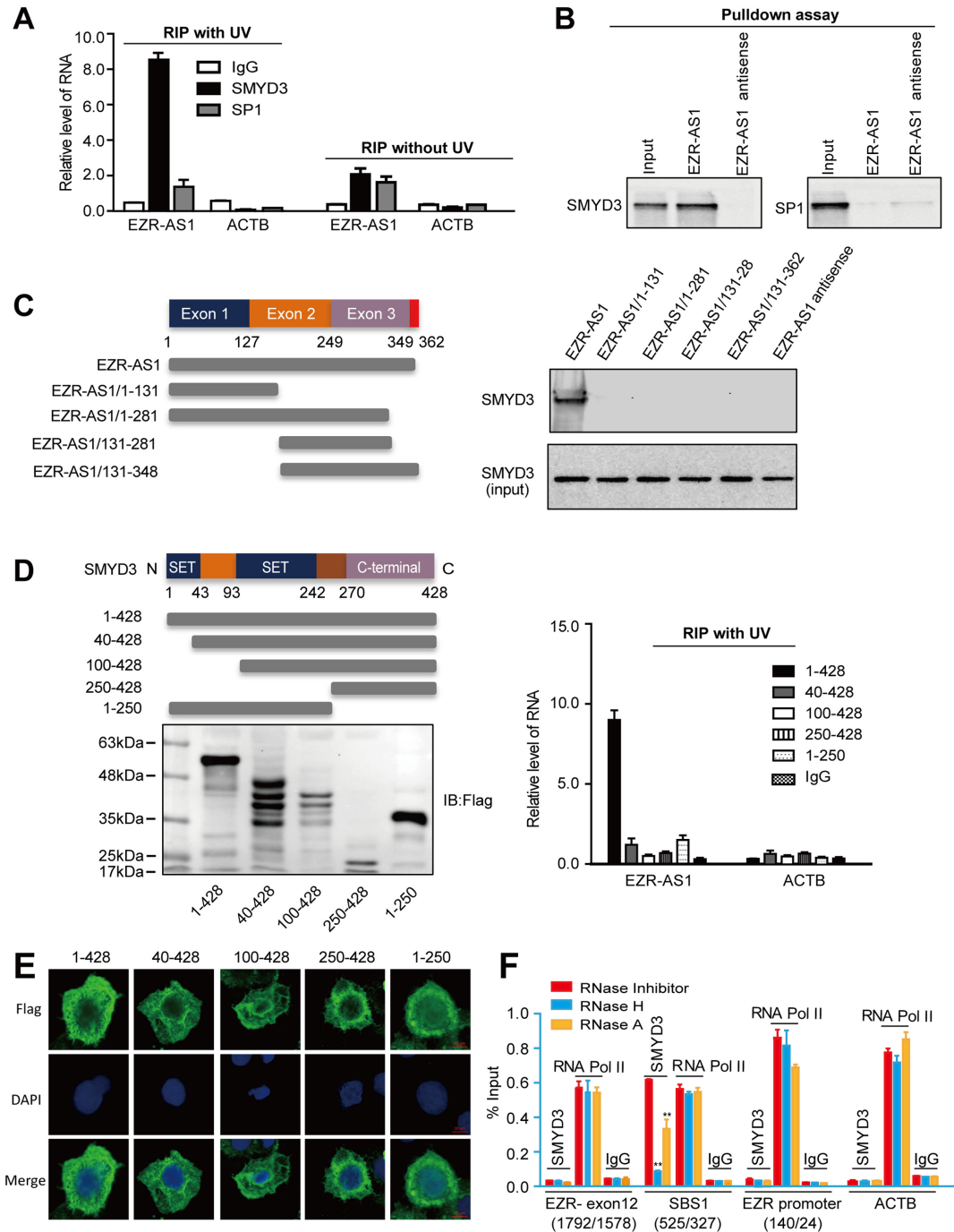


Figure 6. EZR-AS1 recruits SMYD3 via linking SMYD3 to SMYD3 binding sites on the EZR gene. (A) RNA immunoprecipitation (RIP) assay with or without UV irradiation. KYSE150 cells were UV-crosslinked. Then RNA immunoprecipitation was used to detect endogenous EZR-AS1 levels bound to SMYD3 in UV-crosslinked cells or the non-crosslinked cells. IgG, and SP1 antibody was used as negative controls for RIP, whereas ACTB was used as a control for qRT-PCR. Mean \pm SD ($n = 3$). Data were from three independent experiments. * $P < 0.05$ or ** $P < 0.01$. (B) RNA pull-down assay of biotin-labeled full-length EZR-AS1 RNA in KYSE150 cells. Western blot detected SMYD3 in EZR-AS1 complexes. Biotin-labeled EZR-AS1 antisense and SP1 in immunoprecipitates was used as the negative control. Data are representative of three independent experiments. (C) RNA pull-down assay of biotin-labeled full-length EZR-AS1 or truncated EZR-AS1 RNA in KYSE150 cells. Western blot detected bound SMYD3. Data are representative of three independent experiments. (D) RIP assay of truncated SMYD3 in KYSE150 cells. A plasmid encoding Flag-SMYD3 or truncated SMYD3 was transfected into KYSE 150 cells, and an anti-Flag-tag antibody was used to detect expression of all plasmids (*left, down*). Then, the same Flag-tag antibody was used to immunoprecipitate protein-RNA complexes, and EZR-AS1 levels in the immunoprecipitates were determined by qRT-PCR (*right*). (E) Immunofluorescence analysis of Flag-SMYD3. KYSE 150 cells transfected with Flag-SMYD3 or truncated SMYD3 were inoculated onto fibronectin-coated coverslips, and then immunofluorescence analysis was performed. (F) RNase-ChIP assay of anti-SMYD3 or anti-RNA Pol II antibody in permeabilized KYSE150 cells treated with RNase H or RNase A. qPCR was used to detect the amount of EZR genomic DNA. Detection of EZR- exon 12, EZR promoter and ACTB were used as controls. Data (mean \pm SD, $n = 3$) are from three independent transfection experiments. * $P < 0.05$ or ** $P < 0.01$. Data are representative of three independent experiments.

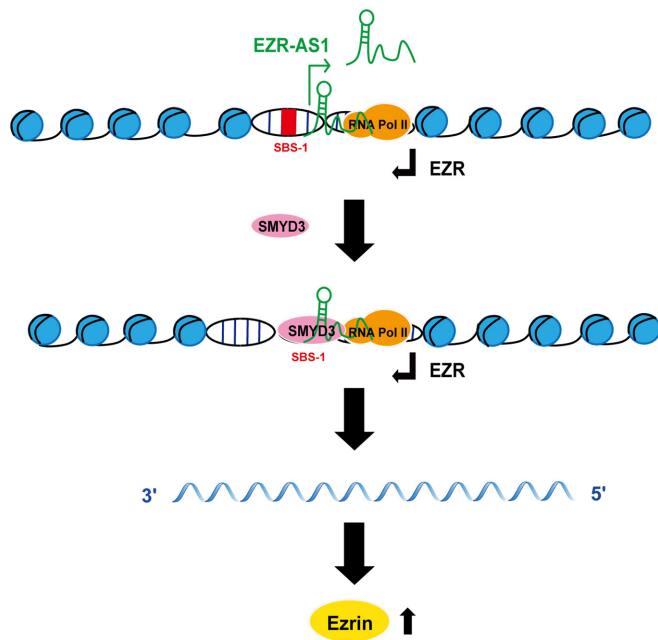


Figure 7. Proposed model for EZR-AS1-mediated enhancement of EZR transcription. Antisense lncRNA EZR-AS1 interacts with RNA polymerase II to activate the transcription of EZR. Simultaneously, EZR-AS1 recruits SMYD3 to a SMYD3 binding site present in the GC-rich stretch downstream of the EZR promoter, causing the binding of SMYD3 and enhanced trimethylation of H3K4. Finally, interaction of EZR-AS1 with SMYD3 further enhances EZR transcription to increase migration of ESCC cells.

tional domains (66). Importantly, ChIP assays show that degradation of EZR-AS1 RNA, by treatment with RNase A or RNase H, causes a total release of SMYD3 from SMYD3-binding site SBS-1, located in the GC-rich region downstream of the EZR promoter (Figure 6F). These results suggest that antisense lncRNA EZR-AS1 may provide a scaffold for SMYD3 recruitment, leading to redistribution and enrichment of SMYD3 along the EZR gene. In addition, since GC-rich regions are generally not conducive to transcription, such recruitment of the histone methyltransferase SMYD3 would be important for triggering chromatin remodeling to enable increased EZR transcription.

The lncRNA ANRASSF1 has been shown to form an RNA/DNA hybrid within its target gene (42), and pRNA (promoter-associated RNA), which is complementary to the rRNA gene promoter, has been found to interact with complementary sequences within the duplex DNA of rDNA, forming an RNA–DNA–DNA triplex structure (67). RNase H digests RNA from RNA/DNA hybrids, but has no effect on single-stranded RNA (ssRNA) or RNA/RNA duplexes, whereas RNase A digests ssRNA, as well as RNA/RNA duplexes (68–72). In our study, we found a 127-nt complementary sequence between the EZR-AS1 RNA and the EZR DNA (Supplementary Figure S1). Treatment of permeabilized cells with RNase H decreases the concentration of endogenous EZR-AS1 (Figure 4H). Furthermore, RNase ChIP assays show that SMYD3 is released from SBS-1 following treatment with RNase H (Figure 6F). These results indicate that RNA–DNA hybrid formation between EZR-AS1 RNA and the EZR DNA may be

involved in EZR-AS1-mediated upregulation of EZR transcription. However, EZR-AS1 RNA–DNA hybrid formation was not directly shown in this study. The formation and mechanisms for RNA–DNA hybrid formation remain to be elucidated in future.

In conclusion, we demonstrate that antisense RNA EZR-AS1 up-regulates EZR transcription and promotes ESCC cell migration through an interaction with both SMYD3 and RNA polymerase II. The highlight of this work is the molecular mechanism by which lncRNAs regulate gene expression whereby EZR-AS1 recruits histone methyltransferase SMYD3 and interacts with RNA polymerase II to promote the transcription of target genes.

SUPPLEMENTARY DATA

Supplementary Data are available at NAR online.

ACKNOWLEDGEMENTS

We thank Dr Stanley Li Lin from the Department of Cell Biology and Genetics of Shantou University Medical College for assistance in revising the manuscript.

FUNDING

Funding for open access charge: National Natural Science Foundation of China [81172264, 81472613, 81772532]; Natural Science Foundation of China-Guangdong Joint Fund [U1301227, U1601229]; National Cohort of Esophageal Cancer of China [2016YFC0901400]; Science & Technology Planning Project of Guang Dong Province [2014A030304060]; Department of Education, Guangdong Government under the Top-tier University Development Scheme for Research and Control of Infectious Diseases. *Conflict of interest statement.* None declared.

REFERENCES

- Yelin, R., Dahary, D., Sorek, R., Levanon, E.Y., Goldstein, O., Shoshan, A., Diber, A., Biton, S., Tamir, Y., Khosravi, R. *et al.* (2003) Widespread occurrence of antisense transcription in the human genome. *Nat. Biotechnol.*, **21**, 379–386.
- Carninci, P., Kasukawa, T., Katayama, S., Gough, J., Frith, M.C., Maeda, N., Oyama, R., Ravasi, T., Lenhard, B., Wells, C. *et al.* (2005) The transcriptional landscape of the mammalian genome. *Science*, **309**, 1559–1563.
- Cheng, J., Kapranov, P., Drenkow, J., Dike, S., Brubaker, S., Patel, S., Long, J., Stern, D., Tammanna, H., Helt, G. *et al.* (2005) Transcriptional maps of 10 human chromosomes at 5-nucleotide resolution. *Science*, **308**, 1149–1154.
- Birney, E., Stamatoyannopoulos, J.A., Dutta, A., Guigo, R., Gingeras, T.R., Margulies, E.H., Weng, Z., Snyder, M., Dermitzakis, E.T., Thurman, R.E. *et al.* (2007) Identification and analysis of functional elements in 1% of the human genome by the ENCODE pilot project. *Nature*, **447**, 799–816.
- Kapranov, P., Cheng, J., Dike, S., Nix, D.A., Dutttagupta, R., Willingham, A.T., Stadler, P.F., Hertel, J., Hackermuller, J., Hofacker, I.L. *et al.* (2007) RNA maps reveal new RNA classes and a possible function for pervasive transcription. *Science*, **316**, 1484–1488.
- Bertone, P., Stolz, V., Royce, T.E., Rozowsky, J.S., Urban, A.E., Zhu, X., Rinn, J.L., Tongprasit, W., Samanta, M., Weissman, S. *et al.* (2004) Global identification of human transcribed sequences with genome tiling arrays. *Science*, **306**, 2242–2246.
- Djebali, S., Davis, C.A., Merkel, A., Dobin, A., Lassmann, T., Mortazavi, A., Tanzer, A., Lagarde, J., Lin, W., Schlesinger, F. *et al.*

- (2012) Landscape of transcription in human cells. *Nature*, **489**, 101–108.
8. Magistri, M., Faghihi, M.A., St Laurent, G. and Wahlestedt, C. (2012) Regulation of chromatin structure by long noncoding RNAs: focus on natural antisense transcripts. *Trends Genet.*, **28**, 389–396.
 9. Faghihi, M.A. and Wahlestedt, C. (2009) Regulatory roles of natural antisense transcripts. *Nat. Rev. Mol. Cell Biol.*, **10**, 637–643.
 10. Numata, K. and Kiyosawa, H. (2012) Genome-wide impact of endogenous antisense transcripts in eukaryotes. *Front. Biosci. (Landmark Ed.)*, **17**, 300–315.
 11. Li, C.H. and Chen, Y. (2013) Targeting long non-coding RNAs in cancers: progress and prospects. *Int. J. Biochem. Cell Biol.*, **45**, 1895–1910.
 12. Jeon, Y. and Lee, J.T. (2011) YY1 tethers Xist RNA to the inactive X nucleation center. *Cell*, **146**, 119–133.
 13. Prensner, J.R., Iyer, M.K., Sahu, A., Asangani, I.A., Cao, Q., Patel, L., Vergara, I.A., Davicioni, E., Erho, N., Ghadessi, M. et al. (2013) The long noncoding RNA SChLAP1 promotes aggressive prostate cancer and antagonizes the SWI/SNF complex. *Nat. Genet.*, **45**, 1392–1398.
 14. Zhao, J., Sun, B.K., Erwin, J.A., Song, J.J. and Lee, J.T. (2008) Polycomb proteins targeted by a short repeat RNA to the mouse X chromosome. *Science*, **322**, 750–756.
 15. Tsai, M.C., Manor, O., Wan, Y., Mosammaparast, N., Wang, J., Lan, F., Shi, Y., Segal, E. and Chang, H.Y. (2010) Long noncoding RNA as modular scaffold of histone modification complexes. *Science*, **329**, 689–693.
 16. Johnsson, P., Ackley, A., Vidarsdottir, L., Lui, W.O., Corcoran, M., Grander, D. and Morris, K.V. (2013) A pseudogene long-noncoding-RNA network regulates PTEN transcription and translation in human cells. *Nat. Struct. Mol. Biol.*, **20**, 440–446.
 17. Su, W.Y., Li, J.T., Cui, Y., Hong, J., Du, W., Wang, Y.C., Lin, Y.W., Xiong, H., Wang, J.L., Kong, X. et al. (2012) Bidirectional regulation between WDR83 and its natural antisense transcript DHPS in gastric cancer. *Cell Res.*, **22**, 1374–1389.
 18. Pelechano, V. and Steinmetz, L.M. (2013) Gene regulation by antisense transcription. *Nat. Rev. Genet.*, **14**, 880–893.
 19. Yang, F., Xue, X., Zheng, L., Bi, J., Zhou, Y., Zhi, K., Gu, Y. and Fang, G. (2014) Long non-coding RNA GHET1 promotes gastric carcinoma cell proliferation by increasing c-Myc mRNA stability. *FEBS J.*, **281**, 802–813.
 20. Bretscher, A., Edwards, K. and Fehon, R.G. (2002) ERM proteins and merlin: integrators at the cell cortex. *Nat. Rev. Mol. Cell Biol.*, **3**, 586–599.
 21. Fievet, B., Louvard, D. and Arpin, M. (2007) ERM proteins in epithelial cell organization and functions. *Biochim. Biophys. Acta*, **1773**, 653–660.
 22. Elzagheid, A., Korkeila, E., Bendardaf, R., Buhmeida, A., Heikkila, S., Vaheri, A., Syrjanen, K., Pyrhonen, S. and Carpen, O. (2008) Intense cytoplasmic ezrin immunoreactivity predicts poor survival in colorectal cancer. *Hum. Pathol.*, **39**, 1737–1743.
 23. Niggli, V. and Rossy, J. (2008) Ezrin/radixin/moesin: versatile controllers of signaling molecules and of the cortical cytoskeleton. *Int. J. Biochem. Cell Biol.*, **40**, 344–349.
 24. Khanna, C., Wan, X., Bose, S., Cassaday, R., Olomu, O., Mendoza, A., Yeung, C., Gorlick, R., Hewitt, S.M. and Helman, L.J. (2004) The membrane-cytoskeleton linker ezrin is necessary for osteosarcoma metastasis. *Nat. Med.*, **10**, 182–186.
 25. Hunter, K.W. (2004) Ezrin, a key component in tumor metastasis. *Trends Mol. Med.*, **10**, 201–204.
 26. Elliott, B.E., Meens, J.A., SenGupta, S.K., Louvard, D. and Arpin, M. (2005) The membrane cytoskeletal crosslinker ezrin is required for metastasis of breast carcinoma cells. *Breast Cancer Res.*, **7**, R365–R373.
 27. Lallemand, D. and Arpin, M. (2010) Moesin/ezrin: a specific role in cell metastasis? *Pigment. Cell Melanoma Res.*, **23**, 6–7.
 28. Meng, Y., Lu, Z., Yu, S., Zhang, Q., Ma, Y. and Chen, J. (2010) Ezrin promotes invasion and metastasis of pancreatic cancer cells. *J. Transl. Med.*, **8**, 61.
 29. Ren, L. and Khanna, C. (2014) Role of ezrin in osteosarcoma metastasis. *Adv. Exp. Med. Biol.*, **804**, 181–201.
 30. Wang, X., Liu, M. and Zhao, C.Y. (2014) Expression of ezrin and moesin related to invasion, metastasis and prognosis of laryngeal squamous cell carcinoma. *Genet. Mol. Res.*, **13**, 8002–8013.
 31. Zhang, Y., Zhang, L., Zhang, G., Li, S., Duan, J., Cheng, J., Ding, G., Zhou, C., Zhang, J., Luo, P. et al. (2014) Osteosarcoma metastasis: prospective role of ezrin. *Tumour Biol.*, **35**, 5055–5059.
 32. Martin, T.A., Harrison, G., Mansel, R.E. and Jiang, W.G. (2003) The role of the CD44/ezrin complex in cancer metastasis. *Crit. Rev. Oncol. Hematol.*, **46**, 165–186.
 33. Zhou, B., Leng, J., Hu, M., Zhang, L., Wang, Z., Liu, D., Tong, X., Yu, B., Hu, Y., Deng, C. et al. (2010) Ezrin is a key molecule in the metastasis of MOLT4 cells induced by CCL25/CCR9. *Leuk. Res.*, **34**, 769–776.
 34. Kishore, R., Qin, G., Luedemann, C., Bord, E., Hanley, A., Silver, M., Gavin, M., Yoon, Y.S., Goukassian, D. and Losordo, D.W. (2005) The cytoskeletal protein ezrin regulates EC proliferation and angiogenesis via TNF-alpha-induced transcriptional repression of cyclin A. *J. Clin. Invest.*, **115**, 1785–1796.
 35. Zhang, X.D., Xie, J.J., Liao, L.D., Long, L., Xie, Y.M., Li, E.M. and Xu, L.Y. (2015) 12-O-Tetradecanoylphorbol-13-acetate induces up-regulated transcription of variant 1 but not variant 2 of VIL2 in esophageal squamous cell carcinoma cells via ERK1/2/AP-1/Sp1 signaling. *PLoS One*, **10**, e0124680.
 36. Jiang, W.G. and Hiscox, S. (1996) Cytokine regulation of ezrin expression in the human colon cancer cell line HT29. *Anticancer Res.*, **16**, 861–865.
 37. Gao, S.Y., Li, E.M., Cui, L., Lu, X.F., Meng, L.Y., Yuan, H.M., Xie, J.J., Du, Z.P., Pang, J.X. and Xu, L.Y. (2009) Sp1 and AP-1 regulate expression of the human gene VIL2 in esophageal carcinoma cells. *J. Biol. Chem.*, **284**, 7995–8004.
 38. Yu, Y., Zeng, P., Xiong, J., Liu, Z., Berger, S.L. and Merlino, G. (2010) Epigenetic drugs can stimulate metastasis through enhanced expression of the pro-metastatic Ezrin gene. *PLoS One*, **5**, e12710.
 39. Zhu, Y., Zhu, M.X., Zhang, X.D., Xu, X.E., Wu, Z.Y., Liao, L.D., Li, L.Y., Xie, Y.M., Wu, J.Y., Zou, H.Y. et al. (2016) SMYD3 stimulates EZR and LOXL2 transcription to enhance proliferation, migration and invasion in esophageal squamous cell carcinoma. *Hum. Pathol.*, **52**, 153–163.
 40. Kent, W.J., Sugnet, C.W., Furey, T.S., Roskin, K.M., Pringle, T.H., Zahler, A.M. and Haussler, D. (2002) The human genome browser at UCSC. *Genome Res.*, **12**, 996–1006.
 41. Li, C.Q., Huang, G.W., Wu, Z.Y., Xu, Y.J., Li, X.C., Xue, Y.J., Zhu, Y., Zhao, J.M., Li, M., Zhang, J. et al. (2017) Integrative analyses of transcriptome sequencing identify novel functional lncRNAs in esophageal squamous cell carcinoma. *Oncogenesis*, **6**, e297.
 42. Beckedorff, F.C., Ayupe, A.C., Crocci-Souza, R., Amaral, M.S., Nakaya, H.I., Soltys, D.T., Menck, C.F., Reis, E.M. and Verjovski-Almeida, S. (2013) The intronic long noncoding RNA ANRASSF1 recruits PRC2 to the RASSF1A promoter, reducing the expression of RASSF1A and increasing cell proliferation. *PLoS Genet.*, **9**, e1003705.
 43. Zeng, F.M., Wang, X.N., Shi, H.S., Xie, J.J., Du, Z.P., Liao, L.D., Nie, P.J., Xu, L.Y. and Li, E.M. (2017) Fascin phosphorylation sites combine to regulate esophageal squamous cancer cell behavior. *Amino Acids*, **49**, 943–955.
 44. Li, L.Y., Xie, Y.H., Xie, Y.M., Liao, L.D., Xu, X.E., Zhang, Q., Zeng, F.M., Tao, L.H., Xie, W.M., Xie, J.J. et al. (2017) Ezrin Ser66 phosphorylation regulates invasion and metastasis of esophageal squamous cell carcinoma cells by mediating filopodia formation. *Int. J. Biochem. Cell Biol.*, **88**, 162–171.
 45. Zou, H.Y., Lv, G.Q., Dai, L.H., Zhan, X.H., Jiao, J.W., Liao, L.D., Zhou, T.M., Li, C.Q., Wu, B.L., Xu, L.Y. et al. (2016) A truncated splice variant of human lysyl oxidase-like 2 promotes migration and invasion in esophageal squamous cell carcinoma. *Int. J. Biochem. Cell Biol.*, **75**, 85–98.
 46. Fang, W.K., Liao, L.D., Li, L.Y., Xie, Y.M., Xu, X.E., Zhao, W.J., Wu, J.Y., Zhu, M.X., Wu, Z.Y., Du, Z.P. et al. (2013) Down-regulated desmocollin-2 promotes cell aggressiveness through redistributing adherens junctions and activating beta-catenin signalling in oesophageal squamous cell carcinoma. *J. Pathol.*, **231**, 257–270.
 47. Schaukowitz, K., Joo, J.Y. and Kim, T.K. (2017) UV-RNA immunoprecipitation (UV-RIP) protocol in neurons. *Methods Mol. Biol. (Clifton, N.J.)*, **1468**, 33–38.
 48. Chen, S., Seiler, J., Santiago-Reichert, M., Felbel, K., Grummt, I. and Voit, R. (2013) Repression of RNA polymerase I upon stress is caused by inhibition of RNA-dependent deacetylation of PAF53 by SIRT7. *Mol. Cell*, **52**, 303–313.

49. Chen, S., Blank, M.F., Iyer, A., Huang, B., Wang, L., Grummt, I. and Voit, R. (2016) SIRT7-dependent deacetylation of the U3-55k protein controls pre-rRNA processing. *Nat. Commun.*, **7**, 10734.
50. Blank, M.F., Chen, S., Poetz, F., Schnolzer, M., Voit, R. and Grummt, I. (2017) SIRT7-dependent deacetylation of CDK9 activates RNA polymerase II transcription. *Nucleic Acids Res.*, **45**, 2675–2686.
51. Tufarelli, C., Stanley, J.A., Garrick, D., Sharpe, J.A., Ayyub, H., Wood, W.G. and Higgs, D.R. (2003) Transcription of antisense RNA leading to gene silencing and methylation as a novel cause of human genetic disease. *Nat. Genet.*, **34**, 157–165.
52. Rinn, J.L., Kertesz, M., Wang, J.K., Squazzo, S.L., Xu, X., Bruggmann, S.A., Goodnough, L.H., Helms, J.A., Farnham, P.J., Segal, E. *et al.* (2007) Functional demarcation of active and silent chromatin domains in human HOX loci by noncoding RNAs. *Cell*, **129**, 1311–1323.
53. Bernstein, E. and Allis, C.D. (2005) RNA meets chromatin. *Genes Dev.*, **19**, 1635–1655.
54. Wang, X., Arai, S., Song, X., Reichart, D., Du, K., Pascual, G., Tempst, P., Rosenfeld, M.G., Glass, C.K. and Kurokawa, R. (2008) Induced ncRNAs allosterically modify RNA-binding proteins in cis to inhibit transcription. *Nature*, **454**, 126–130.
55. Bertani, S., Sauer, S., Bolotin, E. and Sauer, F. (2011) The noncoding RNA Mistral activates Hoxa6 and Hoxa7 expression and stem cell differentiation by recruiting MLL1 to chromatin. *Mol. Cell*, **43**, 1040–1046.
56. Hamamoto, R., Furukawa, Y., Morita, M., Iimura, Y., Silva, F.P., Li, M., Yagyu, R. and Nakamura, Y. (2004) SMYD3 encodes a histone methyltransferase involved in the proliferation of cancer cells. *Nat. Cell Biol.*, **6**, 731–740.
57. Proserpio, V., Fittipaldi, R., Ryall, J.G., Sartorelli, V. and Caretti, G. (2013) The methyltransferase SMYD3 mediates the recruitment of transcriptional cofactors at the myostatin and c-Met genes and regulates skeletal muscle atrophy. *Genes Dev.*, **27**, 1299–1312.
58. Rice, P., Longden, I. and Bleasby, A. (2000) EMBOSS: the European molecular biology open software suite. *Trends Genet.*, **16**, 276–277.
59. Hapgood, J.P., Riedemann, J. and Scherer, S.D. (2001) Regulation of gene expression by GC-rich DNA cis-elements. *Cell Biol. Int.*, **25**, 17–31.
60. Modarresi, F., Faghihi, M.A., Lopez-Toledano, M.A., Fatemi, R.P., Magistri, M., Brothers, S.P., van der Brug, M.P. and Wahlestedt, C. (2012) Inhibition of natural antisense transcripts in vivo results in gene-specific transcriptional upregulation. *Nat. Biotechnol.*, **30**, 453–459.
61. Beltran, M., Puig, I., Pena, C., Garcia, J.M., Alvarez, A.B., Pena, R., Bonilla, F. and de Herreros, A.G. (2008) A natural antisense transcript regulates Zeb2/Sip1 gene expression during Snail1-induced epithelial-mesenchymal transition. *Genes Dev.*, **22**, 756–769.
62. Faghihi, M.A., Modarresi, F., Khalil, A.M., Wood, D.E., Sahagan, B.G., Morgan, T.E., Finch, C.E., St Laurent, G., Kenny, P.J. and Wahlestedt, C. (2008) Expression of a noncoding RNA is elevated in Alzheimer's disease and drives rapid feed-forward regulation of beta-secretase. *Nat. Med.*, **14**, 723–730.
63. Faghihi, M.A., Zhang, M., Huang, J., Modarresi, F., Van der Brug, M.P., Nalls, M.A., Cookson, M.R., St-Laurent, G. and Wahlestedt, C. (2010) Evidence for natural antisense transcript-mediated inhibition of microRNA function. *Genome Biol.*, **11**, R56.
64. Kanduri, C. (2008) Functional insights into long antisense noncoding RNA Kcnq1ot1 mediated bidirectional silencing. *RNA Biol.*, **5**, 208–211.
65. Yamanaka, Y., Faghihi, M.A., Magistri, M., Alvarez-Garcia, O., Lotz, M. and Wahlestedt, C. (2015) Antisense RNA controls LRP1 Sense transcript expression through interaction with a chromatin-associated protein, HMGB2. *Cell Rep.*, **11**, 967–976.
66. Cisse, I., Kim, H. and Ha, T. (2012) A rule of seven in Watson-Crick base-pairing of mismatched sequences. *Nat. Struct. Mol. Biol.*, **19**, 623–627.
67. Schmitz, K.M., Mayer, C., Postepska, A. and Grummt, I. (2010) Interaction of noncoding RNA with the rDNA promoter mediates recruitment of DNMT3b and silencing of rRNA genes. *Genes Dev.*, **24**, 2264–2269.
68. Keskin, H., Meers, C. and Storici, F. (2016) Transcript RNA supports precise repair of its own DNA gene. *RNA Biol.*, **13**, 157–165.
69. Keskin, H., Shen, Y., Huang, F., Patel, M., Yang, T., Ashley, K., Mazin, A.V. and Storici, F. (2014) Transcript-RNA-templated DNA recombination and repair. *Nature*, **515**, 436–439.
70. Keskin, H. and Storici, F. (2015) Defects in RNase H2 stimulate DNA break repair by RNA reverse transcribed into cDNA. *MicroRNA (Sharjah, United Arab Emirates)*, **4**, 109–116.
71. Meers, C., Keskin, H. and Storici, F. (2016) DNA repair by RNA: Templated, or not templated, that is the question. *DNA Repair*, **44**, 17–21.
72. Gupta, R., Chatterjee, D., Glickman, M.S. and Shuman, S. (2017) Division of labor among Mycobacterium smegmatis RNase H enzymes: RNase H1 activity of RnhA or RnhC is essential for growth whereas RnhB and RnhA guard against killing by hydrogen peroxide in stationary phase. *Nucleic Acids Res.*, **45**, 1–14.